REPORT DOCUMENTATION PAGE

Form Approved
OPM No. 0704-0188

Public reporting burden for this collection of information is estimated to average 1 hour per response, including the time for reviewing instructions, searching existing data sources gathering and maintaining the data needed, and reviewing the collection of information. Send comments regarding this burden estimate or any other aspect of this collection of information, including suggestions for reducing this burden, to Washington Headquarters Services, Directorate for Information Operations and Reports, 1215 Jefferson Davis Highway, Suite 1204, Arlington, VA 22202-4302, and to the Office of Information and Regulatory Affairs, Office of Management and Budget, Washington, DC 20503.

1. AGENCY USE ONLY *(Leave Blank)*	2. REPORT DATE 22 August 1997	3. REPORT TYPE AND DATES COVERED Final

4. TITLE AND SUBTITLE
RF-Environment Models for the ADSAM Program

5. FUNDING NUMBERS
N00024-98-D-8124

6. AUTHOR(S)
J. P. Reilly, R. L. McDonald, G. D. Dockery
and J. Stapleton (NSWC/DD)

7. PERFORMING ORGANIZATION NAME(S) AND ADDRESS(ES)
Johns Hopkins University Applied Physics Laboratory
11100 Johns Hopkins Road
Laurel, MD 20723-6099

8. PERFORMING ORGANIZATION REPORT NUMBER
A1A97U-070

9. SPONSORING/MONITORING AGENCY NAME(S) AND ADDRESS(ES)
PEO(TAD)-SC
2531 Jefferson Davis Highway
Arlington, VA 22242-5165

10. SPONSORING/MONITORING AGENCY REPORT NUMBER

19980609 029

11. SUPPLEMENTARY NOTES

12a. DISTRIBUTION/AVAILABILITY STATEMENT
Distribution Statement A – Public Release

12b. DISTRIBUTION CODE

DISTRIBUTION STATEMENT A
Approved for public release;
Distribution Unlimited

13. ABSTRACT *(Maximum 200 words)*

The Air-Directed Surface-to-Air Missile (ADSAM) Program Environmental Working Group (EWG) was tasked with compiling information related to modeling of RF environmental effects on RF sensor systems. The resulting report contains three major sections: "Section A, Monostatic Clutter Models," "Section B, Bistatic Scattering Models," and "Section C, Atmospheric Propagation Models." Section A addresses the spatial, temporal, and frequency characteristics of rain, cloud, sea, land, bird and insect clutter. Section B provides similar information for bistatic scattering from land and sea. Section C addresses refraction, diffraction, absorption and multipath interference.

14. SUBJECT TERMS
ADSAM, Radar Clutter Models, Bistatic Scattering, Atmospheric Propagation

15. NUMBER OF PAGES
81

16. PRICE CODE

17. SECURITY CLASSIFICATION OF REPORT	18. SECURITY CLASSIFICATION OF THIS PAGE	19. SECURITY CLASSIFICATION OF ABSTRACT	20. LIMITATION OF ABSTRACT
Unclassified	Unclassified	Unclassified	SAR

NSN 7540-01-280-5500

Standard Form 298, (Rev. 2-89)
Prescribed by ANSI Std. 239-18
299-01

Figure 5

DTIC QUALITY INSPECTED

A1A97U-070

RF-ENVIRONMENT MODELS FOR THE ADSAM PROGRAM

August 22, 1997

Prepared by

J.P. Reilly, R.L. McDonald, G.D. Dockery,
and J. Stapleton (NSWC/DD)

ABSTRACT

One of the tasks assigned to the Air Directed Surface-to-Air Missile (ADSAM) program Environmental Working Group (EWG) is to prepare text for program documents related to modeling RF environmental effects on sensor systems. This report, prepared in collaboration with EWG participants, contains three major sections : "Section A, Monostatic Clutter Models," "Section B, Bistatic Scattering Models," and "Section C, Atmospheric Propagation Models." Section A addresses the spatial, temporal, and frequency characteristics of the normalized monostatic radar cross section of rain, clouds, sea, land, birds, and insects. The principal author is J.P. Reilly (JHU/APL). It was adapted from an existing clutter guide by the same author : "Monostatic Clutter Models for Naval Radar System Applications" (JHU/APL A3B-97-2-002) dated June 26, 1997. Section B provides similar information for bistatic scattering from land and sea surfaces. The principal author is R.L. McDonald (JHU/APL). Section C addresses atmospheric propagation effects including refraction, diffraction, absorption and multipath interference. The principal authors are G.D. Dockery (JHU/APL) and J. Stapleton (NSWC/DD).

Two items of importance have yet to be adequately addressed by the EWG. The first is site-specific overland clutter models, which are considered to be necessary for realistic performance evaluations of alternative system designs. The models contained in this report are typically generic in nature and are considered suitable for system design studies. Although modeling approaches involving the combination of high fidelity propagation codes and the Digital Terrain Elevation Data (DTED) database are discussed, little work has been done to specify representative sites, scenarios, and terrain characteristics. The second item requiring further study is RF environment models for systems operating at frequencies above 70 GHz, for which very little measurement data and modeling information appears to be available.

ADSAM EWG PARTICIPANTS

ADSAM EWG participants involved in defining the RF environmental models include the following :

M.J. Leumas (EWG chairman),
G.D. Dockery, C.C. Lin, R.L. McDonald,
M.H. Newkirk, and J.P. Reilly
The Johns Hopkins University
Applied Physics Laboratory
Johns Hopkins Road
Laurel, MD 20723

J. Stapleton and P. Adams
Dahlgren Division
Naval Surface Warfare Center
Dahlgren, VA 22448

R. Gabel and M. Ryba
Lincoln Laboratory
Massachusetts Institute of Technology
244 Wood Street
Lexington, MA 02173

J. Hampson
Center for Naval Analyses
4401 Ford Avenue
Alexandria, VA 22302

F. Ganz
Photon Research Associates, Inc.
170 North Country Road
Suite 1
Port Jefferson, NY 11777

A1A97U-070

SECTION A

MONOSTATIC CLUTTER MODELS

Prepared by:

J.P. Reilly
The Johns Hopkins University
Applied Physics Laboratory
Johns Hopkins Road
Laurel, MD 20723-6099

Table of Contents

A.1.0 PURPOSE

The purpose of this section is to define radar clutter models applicable to naval defense systems. The models are chosen to encompass realistic environmental features that potentially have a significant influence on system design and performance.

This presentation is not intended as a comprehensive reference manual on radar clutter. Clutter characteristics are not stated for all possible conditions and parametric trade-offs. There are aspects of radar clutter about which our knowledge is incomplete. Engineering judgment has been used in preparing this document in the interest of completeness. Some descriptions have been simplified to make their application more tractable.

The description of each clutter type is accompanied by a section entitled "commentary and cautionary notes." The commentary section emphasizes major areas of uncertainty, qualification, and general aspects of clutter that are difficult to specify. In cases where such information is applicable, the text has been marked with the asterisk symbol, *. Despite some uncertainties and simplifications, an attempt has been made to include essential features that influence radar design.

The clutter models are generally intended to cover the frequency range from 0.5 to 70 GHz, at both horizontal and vertical polarizations. Some models provide coverage outside this frequency band as indicated in the text. Statistical distributions are predicated on a compressed pulse width greater than 50 ns. In some cases, theoretical models or published data do not cover the full parametric range as needed, and assumptions have been made in the interest of completeness and consistency. Qualifications covering the range of applicability are noted in the commentary sections.

A.2.0   PRECIPITATION CLUTTER

This section presents data applying to various precipitation rates (r). The indicated rate is taken to be the average over a wide-spread "stratiform" rainfall.* Rain rate, and hence average normalized radar cross section, is assumed to vary spatially within the storm as defined by Section A.2.4. The normalized radar cross section varies with time at a given point in space as defined by Section A.2.5. For snow, the precipitation rate is taken as the water content of melted snow.

A.2.1   Spatial Extent

Precipitation is assumed to extend to a maximum diameter of 400 km (216 nmi). The altitude of liquid precipitation is assumed to exist to the bright-band layer (see Section A.2.3.2).* Above the bright-band layer, snow and ice crystals may exist to the tropopause altitude (see Section A.2.3.2.2). The area covered by rain may be centered anywhere within the surveillance region. The maximum range of visibility applicable to non ducting conditions may be determined by a 4/3 earth calculation. During ducting conditions, return power from rain at altitudes within the duct may be visible beyond the 4/3 earth horizon.*

A.2.2   Clutter Return Power

The clutter return power from a single radar resolution cell is directly proportional to the radar cross section of the precipitation contained within the cell. The radar cross section is taken to be the product of the volume of the resolution cell (V_c) and the normalized radar cross section ($\sigma°$) of the precipitation, i.e., the radar cross section area per unit of volume (m^2/m^3). The volume of the resolution cell is determined by the beam width and the range/Doppler resolution capability of the radar. In addition, it may be limited by the vertical extent of the rain.

A.2.3   Normalized Radar Cross Section

A.2.3.1 Below Bright-Band Layer

Below the bright-band layer, the mean value of normalized radar cross section for a particular resolution cell is related to rain rate in the cell and illumination frequency by:

$$\overline{\sigma°} = Kf^4r^{1.6} \ (m^2 / m^3)$$

where f is radar frequency (Hz); r is rain rate (mm/hr); $\overline{\sigma°}$ is the mean value of normalized radar cross section (m^2/m^3) for specific f and r. The constant K has the value

7×10^{-48} for radar frequency below 6.0 GHz, and the value 13×10^{-48} at 35 GHz.* Values for K at other frequencies may be determined by linear interpolation and extrapolation of K against log f.

Table A.2.1 provides examples of normalized radar cross section for various radar frequencies, and for r = 2, 4, and 8 mm/hr.

Table A.2.1 Example of Normalized Radar Cross Section Values for Rain

	$\overline{\sigma}^{\circ}$ (dB m^2/m^3)		
f (GHz)	r=2 mm/hr	4 mm/hr	8 mm/hr
0.5	-118.9	-114.0	-109.2
1.25	-102.7	-98.0	-93.2
3.0	-87.6	-82.8	-78.0
5.6	-76.8	-72.0	-67.2
9.3	-67.0	-62.2	-57.4
17.0	-55.7	-50.9	-46.1
35.0	-42.3	-37.5	-32.7
70.0	-29.5	-24.7	-19.9

A.2.3.2 Bright-Band Layer

A bright-band layer may be assumed to exist in which the values are 10 dB greater than those calculated in Section A.2.3.1.* The bright-band thickness is assumed to be 300 m, * with an upper boundary corresponding to the altitude (h_F) of 0°C isotherm. The normalized radar cross section above the 0°C isotherm is assumed to diminish at a rate of 6.5 dB/km, up to the altitude of the tropopause (h_T).

A.2.3.2.1 Altitude of 0°C Isotherm

The altitude (h_F) of the 0°C isotherm is assumed to be related to latitude (ϕ), according to:

$$h_F = \begin{cases} 4.0 & \text{for } 0 < \phi < 36° \\ 4.0 - 0.075(\phi - 36) & \text{for } \phi \geq 36° \end{cases}$$

where h_F is in km, and ϕ is in degrees.

A.2.3.2.2 Altitude of Tropopause

The altitude of the tropopause (h_T) is assumed to be related to latitude according to:

$$h_T = \begin{cases} 17.0 & \text{for } 0 \le \phi < 30° \\ 9.0 & \text{for } 60° < \phi \le 90° \end{cases}$$

where h_T is in km. Between $\phi = 30°$ and $60°$, h_T may be determined by linear interpolation of height versus latitude.

A.2.4 Spatial Distribution of Rain Rate

The rain rate is assumed to remain constant within a rain cell having length and breadth equal to 2.0 km (1.1 nmi).* Rain rate is assumed to be statistically independent from one rain cell to another. The distribution of rain rate from one rain cell to another is assumed to correspond to a log-normal density function:*

$$p(z) = \frac{1}{\sigma_z \sqrt{2\pi}} \exp(-\beta^2 / 2)$$

where

$$\beta = \frac{z - \mu_z}{\sigma_z}$$

$$z = \log_{10} r$$

$r = $ rain rate

μ_z, $\sigma_z = $ mean, standard deviation of z.

As an example, consider a rain rate with a spatial median equal to 4 mm/hr (log 4 = 0.6), and $\sigma_z = 0.3$ (equivalent to a standard deviation of 3 dB). Accordingly, β is given by:

$$\beta = \frac{z - 0.6}{0.3}$$

Example: $\beta_{50} = 0$; $r_{50} = 4.0$ mm/hr (0.16 in/hr)

$\beta_{84} = 1.00$; $r_{84} = 8.0$ mm/hr (0.32 in/hr)

(in the example, β_{84} means that 84 percent of observations will equal or fall below the stated value.)

A.2.5   Temporal Distribution of Radar Cross Section

The reflected power from a fixed volume resolution cell will vary with time. For time periods up to 80 seconds, the statistical distribution of normalized radar cross section ($\sigma°$) from a fixed volume resolution cell is described by the exponential density function:

$$p\left(\sigma°|\overline{\sigma°}\right) = \frac{1}{\overline{\sigma°}} \exp\left[-\frac{\sigma°}{\overline{\sigma°}}\right]$$

where $p\left(\sigma°|\overline{\sigma°}\right)$ is the probability of $\sigma°$ given $\overline{\sigma°}$, and $\overline{\sigma°}$ is the mean value of normalized radar cross section in the rain cell as defined in Sections A.2.3 and A.2.4.

$\overline{\sigma°}$ is related to the median value of normalized radar cross section in the rain cell, $\sigma°_{50}$, by $\sigma°_{50} = \overline{\sigma°} \ln 2$.

For each period of 80 seconds a new value of $\overline{\sigma°}$ may be assumed in a given volume resolution cell, using the spatial distribution of r given in Section A.2.4.* For example, with a 4 mm/hr rain, the long-term distribution of r in a fixed resolution cell has a median rate of 4 mm/hr (0.16 in/hr), and varies from one 80-second period to another in accordance with the log-normal density function defined in Section A.2.4.

A.2.6   Velocity Distribution

Each volume resolution cell is assumed to be modelled as a many-scatterer process, with a Gaussian distribution of radial components of particle velocities:

$$p(v) = \frac{1}{\sigma_v \sqrt{2\pi}} \exp(-\alpha^2 / 2)$$

where

$$\alpha = \frac{v - v_o}{\sigma_v}$$

v_o, σ_v are the mean and standard deviations.

A.2.6.1 Standard Deviation

The standard deviation of the velocity spectrum (σ_v) can be determined by the root-sum-square of turbulence (σ_t), shear (σ_s), beam broadening (σ_b), and fall (σ_f) components:

$$\sigma_v^2 = \sigma_t^2 + \sigma_s^2 + \sigma_b^2 + \sigma_f^2$$

where

$$\sigma_t = 1.0 \text{ m/s (3.3 ft/s)}$$
$$\sigma_s = 0.42 \text{ k } \Delta h$$
$$\sigma_b = 0.42 \text{ v}_o \, \theta_2 \text{ Sin } \beta$$
$$\sigma_f = F \text{ Sin } \psi$$

k is a shear constant, and Δh is the vertical extent of the two-way 3-dB beam at the resolution cell, within the rain (the elevation extent cannot exceed the maximum rain altitude). The shear constant, k, is equal to 5.0 m/sec/km (5.0 ft/sec/Kft). For Δh expressed in km, $\sigma_s = 2.1 \, \Delta h$ ft/s. V_o is the average wind velocity as defined in Section A.2.6.2, θ_2 is the two-way half-power antenna beamwidth, and β is the angle relative to the mean wind direction. ψ is the antenna elevation angle, and F is the standard deviation of fall velocities. For evaluation purposes, use F = 1.0 m/s (3.28 ft/s).

A.2.6.2 Mean Velocity

The mean scatterer velocity in a volume resolution cell may be calculated using a model that includes a wind velocity of v_s at the surface, 20 m/s (39 knots) at a altitude of 3 km (9.8 kft), 40 m/s (77.6 knots) at an altitude of 10 km (32.8 kft), and 20 m/s (39 knots) at an altitude of 20 km (65.6 kft). Velocity at intermediate altitudes may be determined by linear interpolation of speed versus altitude. The value $v_s = 12$ m/s (23.3 knots) may be considered a relatively large value for the surface wind during a stratiform rain.* The mean fall velocity is assumed to be 10 m/s.

The wind direction may correspond to one of two models. In the first model, the wind direction is constant over the entire elevation extent. In the second model, the wind direction varies at a constant rate of 30° degrees per km of height.

A.2.7 Frequency Correlation

In a fixed resolution cell, back-scattered power is assumed to decorrelate with frequency agility in accordance with a many-scatterer model. Accordingly, the correlation of returned power as a function of frequency change is:

$$\rho(\Delta f) = \left[\frac{\sin \pi \tau \Delta f}{\pi \tau \, \Delta f} \right]^2$$

where τ is the compressed pulse width (sec), Δf is the change in transmit frequency (Hz), $\rho(\Delta f)$ is the correlation coefficient of echo power from two pulses transmitted closely in time, but separated in frequency by the increment Δf. The mean power in a cell and its statistical distribution remains unaffected by frequency agility.

A.2.8 Attenuation

Attenuation refers to a loss by absorption of the propagated signal power relative to free space propagation; it occurs in addition to signal power loss (or gain) from

refractive effects. The attenuation coefficient for rain may be calculated by

$$A = k\, r^{\alpha}$$

where A is the one-way attenuation coefficient (in dB/km), r is rain rate (in mm/h), k and α are coefficients that depend on frequency as listed in Table A.2.2* Values of k and α at other specific frequencies may be determined from the data by interpolation of log f against log k or log α. Table A.2.3 lists example values of attenuation for several frequencies and rain rates.

Table A.2.2 Coefficients for Rain Attenuation Expression

f (GHz)	k	α
1	3.70×10^{-5}	0.896
2	1.46×10^{-4}	0.943
4	6.20×10^{-4}	1.098
6	1.65×10^{-3}	1.287
8	4.24×10^{-3}	1.319
10	9.49×10^{-3}	1.270
15	3.51×10^{-2}	1.141
20	7.21×10^{-2}	1.082
25	0.119	1.046
30	0.177	1.011
40	0.330	0.930
50	0.508	0.921
60	0.525	0.825
80	0.941	0.769
100	1.09	0.743

$A = kr^{\alpha}$ (A = dB/km; r = mm/h)

Table A.2.3 Example Attenuation Coefficient Values for Rain

	Attenuation Coefficient (dB/km)		
f (GHz)	r = 1 mm/hr	r = 4 mm/hr	r = 16 mm/hr
4	6.20×10^{-4}	1.84×10^{-3}	0.013
10	9.49×10^{-3}	0.055	0.321
20	7.21×10^{-2}	0.323	1.45
40	0.330	1.20	4.35
80	0.941	2.73	7.94

A.2.9   Commentary and Cautionary Notes

A.2.9.1   Rain Type

Section A.2.0 roughly defines a widespread stratiform rain. Types of precipitation that may be encountered in a more general context are as follows:

a) Stratiform precipitation - widespread regions with low rain rates and small embedded showers with rain rates up to 25 mm/h. The precipitation is horizontally stratified with rain up to the height of the bright-band (see Section A.2.3.2), with snow to heights of the order of 7 km, and with ice crystals to a height of 9 km.

b) Convection precipitation - localized areas of relatively intense precipitation characterized by strong up - and down-drafts extending through a deep region of the troposphere. The localized regions are columnar in nature sometimes extending to the tropopause. Very intense precipitation may occur with horizontal scales of several kilometers and durations of tens of minutes.

c) Monsoon precipitation - a sequence of bands of intense convection followed by intervals of stratiform precipitation. The bands are typically 50 km across, hundreds of kilometers in length and produce heavy precipitation lasting for several hours.

d) Tropical storms - large organized regions of precipitation extending over hundreds of kilometers. The storms are characterized by several spiral bands terminating in regions of intense precipitation surrounding the central region or eye of the storm. The bands also contain regions of intense convection.

A.2.9.2   Spatial Statistics

Section A.2.4 defines a rain rate statistical model as a log-normal distribution, with a standard deviation of 3 dB. This model is only a rough approximation to the spatial non-uniformity that may be encountered during actual stratiform rains. In Section A.2.5, the same distribution is invoked for a the long-term variation of mean value of normalized radar cross section at a fixed radar resolution cell. The long-term temporal statistical distribution and the spatial distribution are related by the broad scale horizontal velocity of the rainstorm.

A.2.9.3   Spatial Correlation

Section A.2.4 invokes a simple spatial correlation of rate (and therefore mean normalized radar cross section) as either perfectly correlated within a "rain cell," or statistically independent from one cell to another. Spatial scales and correlation patterns may be considerably more variable and complex than the simple model stated here.

A.2.9.4 Bright-Band Layer

In a stratiform rain, an increase in normalized radar cross section may be observed at an altitude band whose upper limit is at the 0°C isotherm. The increase results from differences in particle concentration, shape, and cross section above and below the freezing layer. Increases of roughly 10 dB over liquid rain can be observed within the bright-band layer. The bright-band layer thickness averages approximately 300 m, but can sometimes reach dimensions up to 1 km. The altitude of the bright-band will vary with latitude, climate, and season. The average height of the 0°C isotherm stated in Section A.2.3.2.1 may be taken as the upper boundary of the bright-band during rainy conditions.

A.2.9.5 Frequency Dependence

The relationship stated in Section A.2.3.1 is applicable to Rayleigh scattering in the frequency range below 6 GHz. Above 6 GHz, the particles begin to enter the Mie scattering region. The adjustment of the parameter K approximately compensates for frequency dependence above 6 GHz. Data on frequency dependence of normalized radar cross section within the bright-band was not available for this document.

A.2.9.6 Wind Velocity

The surface wind velocity of 12 m/s cited in Section A.2.6.2 represents a relatively large value that may be encountered during a stratiform rain storm. Over the ocean this value would correspond to a sea-state 5 condition. Surface winds corresponding to other sea states may be approximately determined as described in Section A.4.3.3. Higher surface wind speeds may be encountered during other rain types.

A.2.9.7 Propagation

The joint occurrence of stratiform rain and propagation ducts cannot be precluded on the basis of presently available information. However, we presently lack a rational method for calculation the returned power from near-surface rain within a propagation duct. Such a calculation may require some modification of the assumptions that are customarily made concerning the refractivity profile of clear weather propagation ducts.

A.2.9.8 Attenuation

Attenuation differs slightly at horizontal and vertical polarizations due to the elliptical shape of rain drops. The attenuation coefficients listed in Table A.2.2 are an average of horizontal and vertical polarization values. For critical applications, separate coefficients for horizontal and vertical polarization can be found in CCIR (1986), Section 721-2.

A.3.0 CLOUDS

A.3.1 Spatial Extent

Clouds may exist anywhere throughout the radar surveillance volume, with an altitude extent depending on cloud type as indicated in Table A.3.1 The range visibility of clouds may be determined from a 4/3 earth calculation.

Table A.3.1 Distribution of Clouds

Type	Altitude		Reflectivity Constant (K)	Water Content (g/m³)
	km	kft		
Cirrus	5.0 - 9.0	16.4 - 29.5	6.5×10^{-51}	0.17
Stratocumulus	0.5 - 2.0	1.6 - 6.6	1.6×10^{-50}	0.30
Altocumulus	3.0 - 6.5	9.8 - 21.3	1.6×10^{-50}	0.50
Nimbostratus	0.75 - 4.0	2.5 - 13.1	3.4×10^{-48}	2.0

A.3.2 Clutter Return Power

The clutter return power for clouds is similar to that specified in Section A.2.2 for precipitation. The radar cross section is taken to be the product of the volume of the resolution cell (V_c) and the normalized radar cross section $(\sigma°)$ of the clouds. The maximum height of a radar resolution cell may be limited by the altitude extent of the clouds.

A.3.3 Normalized Radar Cross Section

The median value of the normalized radar cross section, $\sigma°_{50}$, is related to the illumination frequency according to:

$$\sigma°_{50} = K f^4 \quad (m^2 / m^3)$$

The constant K is related to cloud type as indicated in Table A.3.1. Table A.3.2 lists example values of $\sigma°_{50}$ at various radar frequencies.

A1A97U-070

Table A.3.2 Normalized Radar Cross Section for Clouds

Frequency	σ°_{50} (dBm²/m³)		
(Ghz)	Cirrus	Stratocumulus/Altocumulus	Nimbostratus
0.5	-153.9	-150.0	-126.7
1.25	-138.0	-134.1	-110.8
3.0	-122.8	-118.9	-95.6
5.6	-111.9	-108.0	-84.8
9.3	-103.1	-99.2	-75.9
17.0	-92.7	-88.7	-65.5
35.0	-80.1	-76.2	-52.9
70.0	-68.1	-64.2	-40.9

A.3.4   Spatial Distribution of Radar Cross Section

The mean value of normalized radar cross section for clouds is assumed to remain constant over a cell having length and breadth equal to 500 m (0.27 nmi).* The distribution from one cell to another is assumed to be expressed by a log-normal distribution, with a median value as defined in Section A.3.3, and a standard deviation of 5 dB with respect to the median.*

Example: Assume nimbostratus clouds, and f = 1.25 Ghz.

$$\sigma^\circ_{50} = -110.8 \text{ dB m}^2/\text{m}^3$$

$$\sigma^\circ_{84} = -105.8 \text{ dB m}^2/\text{m}^3$$

where σ°_{50} and σ°_{84} are the values below which 50 and 84 percent, respectively, of the observations will fall.

A.3.5   Temporal Distribution of Radar Cross Section

At a fixed resolution cell, the normalized radar cross section is assumed to vary with time according to the exponential distribution as defined in Section A.2.5, but where the variation period of the median value corresponds to 15 sec.*

A.3.6   Velocity Distribution

The mean and standard deviation of the velocity distribution may be determined as described in Section A.2.6,* except that the term σ_f should be ignored.

A.3.7 Frequency Correlation

Frequency correlation is defined in Section A.2.7.

A.3.8 Attenuation

Attenuation is defined in Section A.2.8. The attenuation coefficient for clouds may be calculated for frequencies below 80 Ghz by*

$$A = bWf^{1.93}$$

where A is the attenuation coefficient (in dB/km), W is water content of the cloud (g/m^3) as defined in Table A.3.1, f is radar frequency (Ghz), and b is constant that depends on the temperature of the cloud as follows

$$b = 1.4 \times 10^{-2} \qquad T = -8°C$$

$$b = 1.1 \times 10^{-3} \qquad T = 0°C$$

$$b = 8.3 \times 10^{-4} \qquad T = 10°C$$

$$b = 5.9 \times 10^{-4} \qquad T = 20°C$$

Values of b for other temperatures may be determined by interpolating log b against T. For a stressful case evaluation, T = 0°C is suggested. Examples of attenuation coefficients in clouds are provided in Table A.3.3.

Table A.3.3 Example of Cloud Attenuation Coefficients

Attenuation Coefficient (dB/km)			
f (Ghz)	W=0.25	W=0.5	W=1.0	W=2.0
10	2.34×10^{-2}	4.58×10^{-2}	9.36×10^{-2}	1.87×10^{-1}
20	8.92×10^{-2}	1.78×10^{-1}	3.56×10^{-1}	7.14×10^{-1}
40	3.40×10^{-1}	6.80×10^{-1}	1.36	2.72
80	1.30	2.59	5.18	10.36

W = water content (g/m^3)
T = 0°C

A.3.9   Commentary and Cautionary Notes

A.3.9.1   Spatial Statistics

Section A.3.4 defines a statistical model for normalized radar cross section as a log-normal distribution, with a standard deviation of 5 dB. This model is only a rough approximation to the spatial non-uniformity that may be observed experimentally. Spatial non-uniformities can be expected to be highly variable, exhibiting altitude stratification, and volumetric concentration variations.

A.3.9.2   Spatial Correlation

Spatial scales and correlation patterns may be considerably more complex than the simple model stated in Sections A.3.4 and A.3.5.

A.3.9.3   Wind Velocity

The surface wind velocity referenced in Section A.3.6 is a relatively large value. Over the ocean it corresponds to a sea-state 5 condition. Surface winds corresponding to other sea states may be approximately determined as described in Section A.4.3.3.

A.3.9.4   Attenuation

Attenuation coefficients for frequencies up to 200 GHz are described in CCIR (1986), Report 721-2.

A.4.0 SEA CLUTTER

This section presents methods for calculating sea clutter. Two sections treat the calculation of mean clutter. Section A.4.3 treats calculations for a "standard atmosphere," which is useful as a reference calculation used in Section A.4.4. Section A.4.4 treats sea clutter in the presence of marine boundary evaporation ducts. It requires numerical models for the propagation factor and surface grazing angle under refractivity conditions that differ from the "standard atmosphere".

A.4.1   Spatial Extent

Sea clutter may be assumed to exist at all azimuths up to the 4/3 earth radar horizon in non-ducting conditions. During ducting conditions, sea clutter may be visible at longer ranges, depending strongly on the characteristics of the propagation duct. With surface-based ducts, measurable clutter may be returned from ranges exceeding 200 km.

A.4.2   Clutter Return Power

The clutter return power from a single radar resolution cell is directly proportional to the radar cross section of the sea surface contained within the cell. The radar cross section is taken to be the product of the surface area (A_c) corresponding to the resolution cell and the normalized radar cross section ($\sigma°$) of the surface, i.e., the radar cross section per unit of surface area (m^2/m^2). The surface area of the resolution cell is determined by the beamwidth and the range/Doppler resolution capability of the radar.

A.4.3   Normalized Radar Cross Section : Standard Atmosphere

The equations presented in this section apply to the low grazing angle regime under a "standard atmosphere" propagation condition.* These equations are required to compute the normalized radar cross section under ducting conditions (Section A.4.4).

A.4.3.1 Frequency Range = 0.5 to 10 Ghz

(a)   Mean normalized radar cross section

$$\overline{\sigma°_H} = 10 \log [3.9 \times 10^{-6} \lambda\psi^{0.4} G_a G_u G_w]$$

$$\overline{\sigma°_V} = \begin{cases} \overline{\sigma°_H} - 1.05 \ln (h_a + 0.015) + 1.09\ln(\lambda) + 1.27 \ln (\psi + 0.0001) + 9.70 & \text{(3 to 10 GHz)} \\ \overline{\sigma°_H} - 1.73 \ln (h_a + 0.015) + 3.76\ln(\lambda) + 2.46 \ln (\psi + 0.0001) + 22.2 & \text{(below 3 GHz)} \end{cases}$$

A-14

where $\overline{\sigma^{\circ}_H}$ and $\overline{\sigma^{\circ}_V}$ are the mean values of the normalized radar cross section evaluated at horizontal and vertical polarizations, respectively.

(b) Adjustment factors

$G_a = a^4/(1 + a^4)$

$G_u = \exp\{0.2 \, |\cos \phi| \, (1\text{-}2.8 \, \psi \,)(\lambda +0.015)^{-0.4}\}$

$G_w = [1.94V_w/(1+V_w/15.4)]^q$

(c) Definitions for adjustment factors

$q = 1.1/(\lambda +0.015)^{0.4}$

$a = (14.4 \lambda +5.5) \, \psi \, h_a/(\lambda +0.015)$

A.4.3.2 Frequency Range = 10 to 100 GHz

(a) Mean normalized radar cross section

$\overline{\sigma^{\circ}_H} = 10 \log [5.78 \times 10^{-6} \, \psi^{0.547} \, G_a G_u G_w]$

$\overline{\sigma^{\circ}_V} = \overline{\sigma^{\circ}_H} - 1.38 \ln \left(h_a\right) + 3.43 \ln (\lambda) + 1.31 \ln (\psi) + 18.55$

(b) Adjustment factors

$G_a = a^4/(1 + a^4)$

$G_u = \exp\{0.25 \, |\cos \phi| \, (1 - 2.8 \, \psi \,) \lambda^{-0.33} \}$

$G_w = [1.94V_w/(1+V_w/15.4)]^q$

(c) Definitions for adjustment factors

$q = 1.93 \, \lambda^{-0.04}$

$a = (14.4 \lambda +5.5) \, \psi \, h_a/(\lambda +0.015)$

A.4.3.3 Auxiliary Equations

$h_a = 4.52 \times 10^{-3} V_w^{2.5}$

$V_w = 2.15 \, S^{1.04}$

A-15

A.4.3.4 Units and Symbols

$$\overline{\sigma^{\circ}_{H}}, \overline{\sigma^{\circ}_{V}} = \text{normalized radar cross section for horizontal and vertical polarization (dB m}^2/\text{m}^2)$$

$$h_a = \sqrt{2\pi}\,\sigma_h = \text{average wave height, m}$$

$$\sigma_h = \text{rms wave height, m}$$

$$\lambda = \text{radar wavelength, m}$$

$$\psi = \text{grazing angle, radians}$$

$$V_w = \text{wind velocity, m/s}$$

$$\phi = \text{look direction relative to wind direction, radians}$$

$$S = \text{sea state}$$

A.4.3.5 Grazing Angle

The grazing angle, ψ , may be determined using a standard atmosphere assumption. This is equivalent to a geometric calculation of straight-line propagation over an earth having an equivalent radius $r_e = 1.33\,r_o$, where r_o is the physical earth radius. A minimum value of $\psi = 0.1°$ shall be assumed out to the radar horizon.

A.4.3.6 Nadir Region

In the nadir region ($\psi > 60°$) the mean normalized radar cross section is augmented by specular scattering in accordance with the rms surface slope, $\tan(\beta_o)$,

$$\overline{\sigma^{\circ}}(dB) = 10\log\left\{\exp[-\tan^2(90° - \psi)/\tan^2(\beta_o)]/\tan^2(\beta_o)\right\}$$

where $\tan(\beta_o)$ is defined in Section B.3.1.2.1. In this region the mean value of the normalized radar cross section is taken to be the sum of the low grazing-angle regime contribution, as defined above, and the contribution due to specular scattering.

A.4.4   Normalized Radar Cross Section : Non-Standard Atmosphere

The method presented in this section applies to a non-standard atmosphere, such as subrefractive conditions and surface-based ducts, including evaporation ducts. A ducting condition is typical in marine environments, with evaporation duct heights that vary statistically with season and location. The method described here (after Reilly and

Dockery, 1990) is based on the assumption that the equations presented in Section A.4.3 apply to "standard atmosphere" conditions. The method removes the standard-atmosphere propagation factor from the normalized radar cross section, and substitutes the propagation factor for the specific propagation condition of interest. This results in an adjusted value of normalized radar cross section, $\sigma^{\circ}_{p}(\psi)$, that is calculated as follows:

$$\sigma^{\circ}_{s}(\psi) = \frac{\sigma^{\circ}(\psi)}{F_{s}^{4}[\psi(R)]}$$

$$\sigma^{\circ}_{p}(\psi) = \sigma^{\circ}_{s}(\psi) F_{p}^{4}[\psi(R_{p})]$$

where $\sigma^{\circ}(\psi)$ is the normalized radar cross section determined under standard-atmosphere conditions (Section A.4.3) at the grazing angle ψ, and $F_{s}^{4}[\psi(R)]$ is the propagation factor for a standard atmosphere, evaluated at the range, R, which corresponds to the grazing angle ψ. $F_{p}^{4}[\psi(R_{p})]$ is the propagation factor for the non-standard atmosphere evaluated at the range, R_{p}, which corresponds to the grazing angle ψ. The propagation factors are to be calculated using a high fidelity propagation code (see Section C.7.0). Both $F_{s}^{4}[\psi(R)]$ and $F_{p}^{4}[\psi(R_{p})]$ are evaluated at the effective scattering height of the sea, which is given by $h_{e} = 1.5\sigma_{h}$, where σ_{h} is the rms wave height defined in Section A.4.3.4. $F_{s}^{4}[\psi(R)]$ is calculated assuming an omni-directional antenna pattern, while $F_{p}^{4}[\psi(R_{p})]$ must generally include actual antenna pattern effects.

The grazing angle, $\psi(R_{p})$, for non-standard conditions may be determined using an optical ray-trace computation method. When applying ray-trace methods to a marine boundary layer (MBL) evaporation duct, the slope of the MBL refractivity profile is typically ill-conditioned for ray-trace computations at the surface. Consequently, it is necessary to substitute an adjusted refractivity profile that extrapolates the MBL refractivity determined at h = 0.25 m to the surface along a slope that exists at h = 0.25 m. The ray-trace method will not provide a meaningful solution in skip zones, or in evaporation ducts beyond a critical range, even though a propagation factor may be calculated in those regions. Under some circumstances with strong surface-based ducts, it is possible that a ray-trace solution may return more than one grazing angle at a particular range. This condition can arise when multiple propagation modes create a multi-valued solution at a given range. In such cases, the greatest calculated grazing angle is to be used in the computation model.

A.4.5   Statistical Distribution of Radar Cross Section

The statistical variation of the normalized radar cross section is described here as a compound distribution, in which the value for a fixed radar resolution cell varies in accordance with an exponential distribution whose mean varies from cell to cell according to the Weibull distribution.* In cases where temporal correlation is not of interest, the compound distribution can be approximated as a Weibull distribution with a constant wide-area mean from cell to cell and a larger slope parameter. Alternatively, the

radar cross section varies as defined in Section A.4.7. Discrete clutter is treated as an additional feature. Spatial, temporal, and discrete clutter characteristics are described in Section A.4.6, A.4.7, and A.4.8.

A.4.6 Spatial Distribution of Radar Cross Section

The mean normalized radar cross section is assumed to vary from one radar resolution cell to another in accordance with the Weibull density function:*

$$p(\sigma^\circ) = \frac{\ln 2}{a\,\sigma^\circ}\left(\frac{\sigma^\circ}{\sigma^\circ_{50}}\right)^{1/a} \exp\left[-(\ln 2)\left(\frac{\sigma^\circ}{\sigma^\circ_{50}}\right)^{1/a}\right]$$

where a is the slope parameter and σ°_{50} is the median value of normalized radar cross section across a large number of spatial resolution cells. The cumulative distribution of the normalized radar cross section is given by:

$$P(\sigma^\circ) = 1 - \exp\left[-(\ln 2)\left(\frac{\sigma^\circ}{\sigma^\circ_{50}}\right)^{1/a}\right]$$

The wide-area mean value of the normalized radar cross section, $\overline{\sigma^\circ}$, defined in Section A.4.3, is related to the median value, σ°_{50}, by

$$\frac{\overline{\sigma^\circ}}{\sigma^\circ_{50}} = \frac{\Gamma(1+a)}{(\ln 2)^a}$$

where Γ is the gamma function.

A.4.6.1 Slope Parameter*

The Weibull slope parameter (a) is assumed to related to the resolution cell surface area and grazing angle by:

$\log a = 0.86 - 0.33 \log (A_c \, \psi)$, (for vertical polarization)

$\log a = 1.16 - 0.33 \log (A_c \, \psi)$, (for horizontal polarization)

where A_c is in m^2, and ψ is in degrees.

A.4.6.2 Cumulative Percentile Values

The 90, 99, 99.9, and 99.99 cumulative percentile values of the Weibull variant

are given by:

$$\sigma^{\circ}_{90} = 3.32^{a} \, \sigma^{\circ}_{50}$$

$$\sigma^{\circ}_{99} = 6.64^{a} \, \sigma^{\circ}_{50}$$

$$\sigma^{\circ}_{99.9} = 9.97^{a} \, \sigma^{\circ}_{50}$$

$$\sigma^{\circ}_{99.99} = 13.29^{a} \, \sigma^{\circ}_{50}$$

A.4.6.3 Random Number Generation

Random numbers of the Weibull variate W (σ°_{50},a) can be computed from random numbers of the unit rectangular variate R using the relationship:

$$W\left(\sigma^{\circ}_{50}, a\right) \approx \frac{\sigma^{\circ}_{50}(-\ln R)^{a}}{(\ln 2)^{a}}$$

A.4.6.4 Slope Parameter of Compound Distribution

The compound distribution referred to here consists of an exponential distribution with a Weibull-distributed mean.* The compound distribution itself is approximately Weibull with a slope parameter as indicated in Table A.4.2.

Table A.4.2 Slope Parameter of Compound Distribution

Spatial Distribution	Compound Distribution
0.125	1.03
0.25	1.09
0.5	1.25
1.0	1.64
2.0	2.51
4.0	4.37
8.0	8.19
16.0	16.08
32.0	32.00

Tabulated values indicate the a-parameter of the spatial Weibull distribution, and the a-parameter of the Weibull fit to the compound distribution.

A.4.7 Temporal Distribution of Radar Cross Section*

For a fixed radar resolution cell, the radar cross section is assumed to fluctuate over short time intervals (t << ls) with a distribution following the exponential density function as specified in Section A.2.5, and with a fluctuation spectrum derived from the velocity distribution specified in Section A.4.9. For long-term observations (t ~ 1 s), the mean power in a fixed resolution cell is assumed to slowly vary, and will exhibit a long-term statistical distribution in accordance with the Weibull distribution defined in Section A.4.6. The temporal scale of this slow fluctuation will be roughly periodic on a time scale consistent with the period of the significant sea waves (about 1 to 10 s over the range of sea states from 1 to 6).

A.4.8 Discrete Sea Clutter*

In addition to distributed clutter from the surface, the radar return from the sea may contain echoes from large man-made objects including oil drilling platforms, ships, and buoys, as well as naturally occurring discrete returns known as sea spikes. The radar cross section of these discrete clutter sources may range in size from 0 to more than 60 dBm^2. Man-made objects will be modeled as point reflectors of constant radar cross section. The average density of these reflectors in a littoral environment is assumed to be inversely proportional to the radar cross section, as follows; one 40 dBm^2 reflector per 2.6 km^2 (1.0 mi^2), one 50 dBm^2 reflector per 26 km^2 (10 mi^2), and one 60 dBm^2 reflector per 260 km^2 (100 mi^2).

Sea spikes are considered to arise from physical processes having dimensions that are smaller than the smallest practical radar resolution cell. At Sea State 5, for example, type A sea spikes are assumed to be present with an average density of one reflector per 2 km^2 (0.58 nmi^2); type B sea spikes are present with an average density of one per 60 km^2 (17.5 nm^2). At X-band (9.3 GHz) and Sea State 5, the radar cross section of each spike is assumed to be 10 dBm^2 for type A, and 20 dBm^2 for type B. At other radar frequencies, the sea spike radar cross section is to be scaled relative to the X-band value, $\sigma_{9.3\,GHz}$, as follows,

$$\sigma_f = \sigma_{9.3\,GHz} + 24.4\log(f) - 23.6 \quad dBm^2, \quad f \leq 12.5\,GHz$$

$$= \sigma_{9.3\,GHz} + 3.25\log(f) - 0.40 \quad dBm^2, \quad f > 12.5\,GHz$$

For example, at 5.6 GHz, the type A sea spike radar cross section is 4.7 dBm^2. The radar cross section is assumed vary in direct proportion to sea state with an incremental change of 5 dB per sea state.

Sea spikes are assumed to exist with a lifetime of 4 s with vertical polarization, and 2 s with horizontal polarization. During their lifetime, sea spikes fluctuate in power in accordance with the exponential density function defined in Section A.2.5, and with spectral characteristics consistent with the velocity distribution defined in Section A.4.9.

A.4.9   Velocity Distribution

Each resolution cell may be modeled as a many-scatterer process, with a Gaussian distribution of particle velocities as specified in Section A.2.6.*

A.4.9.1   Standard Deviation of Velocity Spectrum

The standard deviation of the velocity spectrum (σ_v) is related to wind velocity in accordance with:

$$\sigma_v = 0.23 \, V_w \, (m/s)$$

where V_w is the wind velocity in m/s. The relationship between sea state and wind velocity is expressed in Section A.4.3.3.

A.4.9.2   Mean Velocity

The mean velocity of the clutter attains a maximum value when the radar azimuth is aligned with the wind direction in accordance with

$$V_d = \begin{cases} 0.85 \, V_w^{0.5} \, \text{Cos} \, \phi \text{ (horizontal polarization)} \\ 0.15 \, V_w \, \text{Cos} \, \phi \text{ (vertical polarization)} \end{cases}$$

where V_d is the mean Doppler velocity (m/s), V_w is the wind velocity (m/s), and ϕ is the radar azimuth with respect to the wind direction. The relationship between wind velocity and sea state is given in Section A.4.3.3.

A.4.10   Frequency Correlation

In a fixed-resolution cell, the back-scattered power is assumed to decorrelate with frequency agility in accordance with a many-scatterer model, as described in Section A.2.7. The mean power in a cell and its statistical distribution remains unaffected by frequency agility. The back-scattered power from discrete returns, including sea spikes, is also assumed to remain unaffected by frequency agility.

A.4.11   Commentary and Cautionary Notes

A.4.11.1 Grazing Angle

The grazing angle adjustment has been frozen to a minimum angle at a point approximately consistent with the interference region range limit. Experimental verification of a grazing angle adjustment is complicated by the lack of reliable data at shallow grazing angles.

A.4.11.2 Statistical Distribution of Radar Cross Section

The statistical models (Sections A.4.5 to A.4.7) may be interpreted as a "compound distribution," i.e., Rayleigh in a fixed-resolution cell for short-time periods, and having a mean that varies on a longer term basis according to a Weibull distribution. Other studies have postulated a compound distribution in which the mean power varies according to a chi-square distribution. The Weibull distribution has been used in this document because it is relatively simple to use for analysis or simulations.

The specified compound distribution will converge to the Rayleigh-Power (exponential) function as the illuminated area and grazing angle are increased, and will become more skewed (spiky) as the illuminated area and grazing angle are decreased. While this trend conforms to experimental observations, a precise functional relationship is speculative at this time. Relevant parameters will include the illuminated area grazing angle, wavelength, sea conditions, wind direction, and polarization.

The specified Weibull slope parameter relationship (Section A.4.6.1) has been adapted from X-band data that were originally analyzed for vertical polarization in terms of the chi-square distribution. The specified slope parameter for horizontal polarization represents a rough attempt to account for the more spiky distribution reported for horizontal polarization as compared with vertical polarization.

A.4.11.3 Discrete Sea Clutter

Data published by Lin (1996) characterizing radar experience in the Persian Gulf and Red Sea indicates that off-shore oil fields and other man-made objects can cause significant radar returns. Little data exists on the density and size of man-made seaborne discrete clutter sources. The discrete clutter model included in Section A.4.8 was suggested in Skolnik (1990). It is probably more representative of land-based discrete reflectors, and is considered a conservative sea-based model for littoral environments. Of course, man-made discrete returns would be far fewer under open-ocean conditions.

High-resolution radar sea clutter will exhibit resolution cells that have radar cross section levels well above the mean, and that maintain the appearance of a physical entity for long periods (1-5 sec.). Relevant variables affecting the characteristics of these "sea spikes" will include the size of the illuminated area, sea conditions, look direction, wavelength, grazing angle, and polarization. At the present time, we lack a consistent model for sea spikes that takes into account relevant radar and sea variables. The sea spike density and magnitude specified in Section A.4.8 are roughly based on limited data at X-band. The cited X-band values, and the methods for extrapolation to other radar frequencies are speculative due to the lack of appropriate measurements. Available data are inadequate to provide guidance on the sea state dependence of sea spikes.

The specified sea spike amplitude and density are not necessarily consistent with the statistical distribution specified in Section A.4.5. At the present time, we lack a model for sea clutter that describes the pertinent radar observables in a consistent manner.

A.4.11.4 Temporal and Spatial Correlation

In order to keep the clutter description tractable, the specified sea clutter model invokes very simple spatial and temporal correlation statements. Sea clutter spatial correlation patterns will be evinced as much more complex range and azimuth patterns of radar cross section that correlate with sea features, including wave and swell patterns, breaking waves, and wind-blown spray. Temporal patterns of radar cross section in a fixed resolution cell will follow from the spatial patterns and wave velocity. It is likely that sea spikes also correlate with sea features, and exhibit some degree of spatial regularity, although available data are insufficient for a quantitative model.

A.4.11.5 Spectrum

The spectrum standard deviation may be determined from the velocity distribution (Section A.4.9.1) which is based on an overall trend of data collected under a variety of radar and sea conditions. More complex relationships have been studied in terms of grazing angle, wind and wave conditions, and polarization. We presently lack a spectrum model that is valid for all relevant radar and sea conditions.

In accordance with generally accepted practices, the spectrum shape has been specified in terms of the Gaussian function (Section A.4.9). There is some evidence for sea clutter spectral distributions having tails that fall off more slowly than the Gaussian model.

It is generally accepted that sea spikes scintillate in amplitude, despite their temporal persistence as a physical entity. The specification model states that the spike scintillation spectrum and mean velocity correspond to the general background clutter. There are suggestions that the scintillation spectrum of sea spikes may actually be broader, and the mean Doppler offset lower than the general background, but these indications are not presently well established.

Data relating to the mean velocity are not well documented. The description in Section A.4.9.2 is based on relatively little data published in Nathanson et al. (1991).

A.4.11.6 Sea State

The sea clutter model described here uses "sea state" as a convenient and familiar index of sea conditions. The sea parameter relationships are approximations that apply to the open ocean in which the wind has been blowing at a constant velocity for an unlimited time and over an unlimited fetch. In any practical situation, both duration and fetch will be limited, the wind will not have a constant velocity, and shoreline wave interactions may be present.

A.5.0 LAND CLUTTER

An adequate model of land clutter effects for radar performance analysis requires a site-specific model, such as the RADSCAT model described by Reilly and Lin (1995). That model provides the magnitude and spatial distribution of land clutter under specific conditions of meteorology. Generic analytic models do not adequately address the characteristics of land clutter needed for an accurate assessment of radar performance in most instances. However, a generic model can be useful in satisfying limited objectives.

This section provides a simple generic land clutter model which is intended for limited purposes. One can use the generic model to determine the expected dynamic range of clutter, and the maximum spatial extent of the clutter. In addition, a number of characteristics defined in the generic model are needed to augment the site specific model as cited above. These include the statistical treatment of mean clutter values (Section A.5.4 and A.5.5) temporal aspects (Section A.5.6), and the frequency agility response (Section A.5.9). It is not recommended that the clutter model described here be used as the sole descriptor of land clutter when accurate modeling of radar performance is required.

A.5.1 Spatial Extent

Maximum terrain altitude is assumed to be 2 km (6560 ft) in high relief and 0.2 km (656 ft) in low relief environments. The average terrain slope from shore to peak is assumed to be 7° in high relief and 2° in low relief areas.

Land clutter is assumed to be visible within a band that depends on terrain relief, radar distance to shore, and propagation condition in accordance with Section A.5.3.3. Within the region of visibility, land clutter will have a patchy appearance, with shadowed regions interspersed with illuminated regions. The elevation angle needed to illuminate radar-visible terrain will also vary with terrain relief, radar distance to shore, and propagation condition in accordance with Section A.5.3.4.

A.5.2 Clutter Return Power

The clutter return power from a single radar resolution cell is directly proportional to the radar cross section of the terrain surface contained within the cell. The radar cross section is taken to be the product of the surface area (A_c) corresponding to the resolution cell and the normalized radar cross section ($\sigma°$) of the surface, i.e., the radar cross section per unit of surface area (m^2/m^2). The surface area of the resolution cell is determined by the beamwidth and the range/Doppler resolution capability of the radar.

A.5.3   Normalized Radar Cross Section

A.5.3.1   Low-Medium Grazing Angle Region

The wide-area mean value of the normalized radar cross section at X-Band (9.3 GHz) for various terrain types is defined below for grazing angles from 0° to 10° where the grazing angle is taken with respect to a smooth earth. For grazing angles above 10°, increase $\overline{\sigma}^{\circ}_{9.3\,GHz}$ by the factor $10 \log 0.1\,\psi$, where ψ is the smooth earth grazing angle (degrees).

$\overline{\sigma}^{\circ}_{9.3\,GHz}$ = -10 dB for urban areas and other precipitous terrain types

$\overline{\sigma}^{\circ}_{9.3\,GHz}$ = -20 dB for high relief terrain

$\overline{\sigma}^{\circ}_{9.3\,GHz}$ = -30 dB for low relief terrain

The mean value is the average taken over illuminated cells. At other radar frequencies the mean normalized radar cross section is given by

$$\overline{\sigma}^{\circ}(dB) = \overline{\sigma}^{\circ}_{9.3\,GHz}, \qquad\qquad f \le 9.3\ GHz$$

$$\overline{\sigma}^{\circ}(dB) = \overline{\sigma}^{\circ}_{9.3\,GHz} + 5 \log (f/f_0), \qquad f > 9.3\ GHz$$

where $\overline{\sigma}^{\circ}_{9.3\,GHz}$ is the mean value at X-band, f is the radar frequency in GHz, and $f_0 = 9.3$ GHz. Table A.5.1 summarizes the wide-area mean values for the three terrain types at various frequencies at X-band and above. These values are conditioned on having illuminated terrain within the radar resolution cell.

Table A.5.1 Mean Normalized Radar Cross Section of Terrain

Frequency (GHz)	Mean Normalized Radar Cross Section (dBm^2/m^2)		
	Urban	High Relief	Low Relief
9.3	-10.0	-20.0	-30.0
17.0	-8.7	-18.7	-28.7
35.0	-7.1	-17.1	-27.1
70.0	-5.6	-15.6	-25.6

Values indicate mean normalized radar cross section taken over a large area of illuminated terrain. Values apply to grazing angles in the range 0° to 10° with respect to a smooth earth.

A.5.3.2 Nadir Region

In the nadir region ($\psi > 40°$) the mean normalized radar cross section is augmented by specular scattering in accordance with the rms surface slope, $\tan(\beta_o)$,

$$\overline{\sigma°}(dB) = 10\log\{0.65\exp[-\tan^2(90° - \psi)/\tan^2(\beta_o)]/\tan^2(\beta_o)\} + 5\log(f/f_o)$$

where

$$\begin{aligned}\tan(\beta_o) &= 0.2 \quad \text{for urban areas} \\ &= 0.55 \quad \text{for high-relief terrain} \\ &= 0.14 \quad \text{for low-relief terrain.}\end{aligned}$$

In this region the mean value of the normalized radar cross section is taken to be the sum of the low grazing-angle regime contribution, as defined above, and the contribution due to specular scattering.

A.5.3.3 Inclusion of Propagation Factor

Calculations of returned radar power include the two-way propagation factor F^4, for which simplified approximations are listed below.

A.5.3.3.1 For Standard Atmosphere Propagation

Assume $F^4 = 1$ at all distances and altitudes for radar cells containing illuminated terrain. Terrain is considered illuminated to a maximum range given by the following equation:

$$R_h = 4.12 \, (h_a^{1/2} + h_p^{1/2})$$

where R_h is the maximum horizon range (km) in a standard atmosphere, h_a is the antenna height (m), and h_p is the peak altitude (m) of the terrain. Assume $F^4 = 0$ for all ranges beyond R_h. The minimum illuminated terrain range R_0 can be determined using the terrain slope and peak given in Section A.5.1, along with a horizon range calculation. For purposes of determining terrain visibility, assume a low relief environment for urban areas and a high relief environment for other precipitous terrain types.

A.5.3.3.2 For an Atmosphere Having a Duct

Define F_d^4 as the two-way propagation factor for a smooth earth at an altitude that is 1/2 the duct height. Determine F_d^4 to a maximum range from the radar given by:

$$R_d = R_s + 0.55 \, h_d$$

where R_d is the maximum ducted visibility range (km), R_s is range from radar to shore (km), and h_d is the duct height (m). Calculate F_d^4 using a high fidelity propagation model (see Section C.7.0) which includes the refractive effects of the duct. Assume that

evaporation ducts terminate at 2 km (1 nmi) inland from the coast and a standard atmosphere condition prevails thereafter.

R_0 and R_h (Section A.5.3.3.1) indicate the band of land that would be visible without ducting. When ducting is present, contributions from the illuminated band (R_s to R_d) are considered in addition to those visible without ducting. Between R_0 and R_h, assume $F_d^4=1$. Between R_s and R_d, assume the calculated value of F_d^4 discussed above. In the region where these two bands overlap, use the greater of the two values. Outside the visible regions, assume that $F_d^4=0$.

A.5.3.4 Elevation Coverage

Under standard atmosphere conditions, the maximum elevation angle needed to illuminate terrain may be calculated using the peak terrain height specified in Section A.5.1 along with a standard atmosphere assumption. Under ducting conditions, the maximum elevation angle supporting propagation within the duct may be assumed to be less than 1°. For propagation outside the duct, a standard atmosphere calculation may be used to determine elevation.

A.5.4 Statistical Distribution of Radar Cross Section

The statistical variation of the normalized radar cross section among illuminated cells is described here as a compound distribution, in which the value for a fixed radar resolution cell varies in accordance with an exponential distribution whose mean varies from cell to cell according to the Weibull distribution.* In cases where temporal correlation is not of interest, the compound distribution can be approximated as a Weibull distribution with a constant wide-area mean from cell to cell and a larger slope parameter. Alternatively, the radar cross section varies as defined in Section A.5.6. Discrete clutter is treated as an additional feature. Spatial, temporal, and discrete clutter characteristics are described in Section A.5.5, A.5.6, and A.5.7.

A.5.5 Spatial Distribution of Radar Cross Section

For grazing angles less than 10° the mean normalized radar cross section is assumed to vary from one radar resolution cell to another in accordance with the Weibull density function defined in Section A.4.6. The Weibull slope parameter, a, is given by

$$a = 6.74 - 0.8 \log A_c \quad \text{for low relief terrain and urban areas,}$$
$$= 3.05 - 0.28 \log A_c \quad \text{for high relief and precipitous terrain,}$$

where A_c is the area of the resolution cell (in units of m²). The mean value of the Weibull distribution is defined in Section A.5.3. For grazing angles greater than 10° the mean normalized radar cross section remains constant from cell to cell as defined in Section A.5.3.

In cases where temporal correlation is not of interest, the wide-area distribution of instantaneous normalized radar cross section can be modeled as a Weibull distribution

with compound a-parameter specified in Table A.4.2, and mean value specified in
Section A.5.3.

A.5.6 Temporal Distribution of Radar Cross Section

For a fixed resolution cell, the back-scattered power is assumed to fluctuate over
time with a statistical distribution following the exponential density function as specified
in Section A.2.5 and with a fluctuation spectrum derived from the velocity distribution
specified in Section A.5.8. The mean value for a fixed resolution cell is determined by the
spatial distribution specified in Section A.5.3.

A.5.7 Discrete Clutter*

In addition to distributed clutter from terrain surfaces, the radar return from land
may contain echoes from large man-made objects including buildings, towers, and
bridges. The radar cross section of these discrete clutter sources may range in size from
30 to more than 60 dBm^2. These large, rigid structures can be modeled as point reflectors
with constant radar cross section. The average density of these reflectors is assumed to
be inversely proportional to the radar cross section, as follows; one 40 dBm^2 reflector per
2.6 km^2 (1.0 mi^2), one 50 dBm^2 reflector per 26 km^2 (10 mi^2), and one 60 dBm^2 reflector
per 260 km^2 (100 mi^2). The return may also include echoes from moving vehicles with
Doppler velocities corresponding to vehicular speeds. These range in size from 2 to 200
m^2. The occurrence of vehicle reflections will be highly variable, depending on local
terrain and cultural features.

A.5.8 Velocity Distribution

The return for each resolution cell can be modeled as a many-scatterer process,
with a Gaussian distribution of particle velocities as specified in Section A.2.6, and with
zero mean. The standard deviation of velocity spectrum is assumed to be 0.6 m/s (2.0 ft/s)
for low relief environments, 0.3 m/s (1.0 ft/s) for high-relief environments, and 0 for
urban environments.

A.5.9 Frequency Correlation

In a fixed-resolution cell, the back-scattered power is assumed to decorrelate
with frequency agility in accordance with a many-scatterer model, as described in Section
A.2.7, except for the 0.1 percentile strongest reflecting cells, which do not decorrelate
with frequency agility. The mean power in a cell and its statistical distribution remain
unaffected by frequency agility. The back-scattered power from discrete clutter sources
is also assumed to remain unaffected by frequency agility.

A-28

A.5.10 Commentary and Cautionary Notes

A.5.10.1 Land Clutter Types

The great diversity of land types and man-made development makes it extremely difficult to characterize land clutter on a simple, meaningful scale. Important variables will include terrain contours, vegetation, moisture content, and the presence of man-made objects. The specifications listed in Section A.5.0 present gross characterizations of land.

A.5.10.2 Shadowing

Terrain shadowing at low grazing angles can be significant. As the radar resolution cell is made smaller, the fraction of shadowed land clutter cells will increase, especially in irregular terrain. The resulting "holes" in the land return can present the opportunity for detection and tracking of airborne targets. For simplicity, the models defined in Sections A.5.1 and A.5.3.3 give land visibility within a band, without specifying shadowing structure. When analyzing a signal processing scheme that depends on spatial visibility structure, it is advisable to use more detailed models that provide such structure, such as (Reilly and Lin, 1995).

A.5.10.3 Grazing Angle Dependence

The model defined in Section A.5.3.1 for normalized radar cross section is independent of grazing angle for grazing angles less than $10°$. Grazing angle, ψ, is defined here as the angle between a propagating ray and the local terrain slope. Except for very low relief terrain, grazing angles will be dominated by terrain slopes, and will be relatively little affected by the incident angle of propagating energy. Average terrain slopes will depend primarily on the classification of terrain relief, the effects of which are incorporated in Section A.5.3.1. Experimental data is sometimes reported as being dependent on ψ^n, with n ranging from 0 to 1. Some investigators have reported normalized radar cross section as dependent on the depression angle of the radar, rather than grazing angle (Billingsley, 1993).

A.5.10.4 Frequency Dependence

Interpretations of experimental data may be found suggesting that the normalized radar cross section varies with frequency as f^n with values of n ranging from 0 to 1. One investigator (Billingsly, 1993) indicates that the normalized radar cross section for some terrain classifications decreases with increasing frequency below X-band. A popular reference (Nathanson et al., 1991) suggests using the value $n = \frac{1}{2}$ for all frequencies from UHF through W-band. Section 5.3 specifies a value of $n = 1/2$ for frequencies at X-band and above. However, for the sake of conservatism, the normalized radar cross section is assumed to remain constant at the X-band value for frequencies

below X-band. This assumption is consistent with measurements made by Billingsly (1993) for most terrain classifications at grazing angles exceeding one degree.

A.5.10.5 Propagation Factor

There are many uncertainties concerning the modeling of coastal propagation, including the land/sea interface and the interaction of terrain with meteorology characteristics. The models provided in Section A.5.3.3 are thought to provide simple representations of coastal propagation that adequately capture conditions that are stressful to radar performance, and can be physically justified under some conditions.

Calculations of returned power include the two-way propagation factor F^4. Recent high-fidelity models calculate F^4 as a function of range and altitude at each azimuth from the radar, using the terrain height contour (determined from the Defense Mapping Agency "DTED" data base) as an absorbing boundary condition (Reilly and Lin, 1995). As an alternative, Section A.5.3.3.2 provides a simplified procedure for the analyst who lacks the appropriate facilities for such high fidelity calculations. The assumption here is that $F = 1$ for non-ducted illumination of terrain.

Propagation within a surface-based duct can occur over long distances through downward refraction at the upper limit of the duct, and upward reflection from the sea. Repeated application of this mechanism can propagate energy for long distances over the sea. Propagation inland via this mechanism will be limited, however, because of absorption and diffuse scattering at the terrain surface. Section A.5.3.3.2 assumes propagation to an inland distance roughly equal to one surface convergence distance (R_d) for a surface-based duct. It is assumed that a surface-based duct over the sea can follow the land contour under a sea breeze.

Propagation within an evaporation duct can enhance the propagation of energy at low altitudes. Once inland, the humidity gradient responsible for an evaporation duct will dissipate. Specification 5.3.3.2 provides a rough estimate of the limits of inland propagation under evaporation ducts with a sea breeze.

A.5.10.6 Statistical Distribution of Radar Cross Section

The spatial statistics have been defined in terms of the Weibull distribution. It is anticipated that the slope parameter will depend on a variety of variables related to the radar and the terrain. The relationship listed in Section A.5.5 represents an attempt to include the effects of illuminated area; in addition, other parametric dependencies may also be important, including grazing angle, frequency, and terrain characteristics. We presently lack a model that accounts for all relevant parameters.

A.5.10.7 Temporal Distribution of Radar Cross Section

Reflections from wind-blown vegetation will produce a time-varying echo from a fixed land clutter cell. The land echo amplitude is frequently represented as a Rice distribution (single steady reflector plus a random array). For simplicity, the model cited

in Section A.5.6 is based on the assumption that the steady component is not present. This represents a somewhat conservative assumption for radar performance calculations.

A.5.10.8 Discrete Clutter

Little data exists on the density and size of man-made discrete clutter sources. Significant variations may be anticipated depending on the scale of cultural development. The discrete clutter model included in Section A.5.7 was suggested in Skolnik (1990). It is considered to be more representative of metropolitan areas and is, therefore, a conservative model for rural environments.

A.6.0 BIRD CLUTTER

A.6.1 Spatial Extent

Birds are assumed to be distributed from the minimum to the maximum instrumented range, over 360° Azimuth, and within a layer having a vertical extent of 300 m (984 ft). The altitude of this layer is assumed to be anywhere between a minimum and a maximum value that depends on the migration type as follows:

A. Heavy migration: 0.3 - 6.0 km (1 - 19.7 kft)

B. Light migration: 0.3 - 6.0 km (1 - 19.7 kft)

C. Non-migratory: 0 - 3.0 km (0 - 9.8 kft)

(The terms "heavy" and "light" apply to population density, rather than bird size.) The maximum visible range extent may be determined by the maximum bird altitude, and a 4/3 earth calculation during "standard atmosphere" conditions. During ducting conditions, low flying birds within the duct may be seen beyond the optical horizon. The propagation loss for low flying birds may be calculated in the same manner as used for radar targets.

A.6.2 Clutter Return Power

The clutter return power from a single radar resolution cell is directly proportional to the total radar cross section of the birds contained within the cell. The number of birds within a cell is statistically derived based on the average spatial distribution (number per unit area) of the bird population and the surface area (A_c) corresponding to the resolution cell. The surface area of the resolution cell is determined by the beamwidth and the range/Doppler resolution capability of the radar.

A.6.3 Radar Cross Section

When more than one bird is in a resolution cell, the average radar cross section is defined by

$$\overline{\sigma^\circ} = n\, \overline{\sigma^\circ_B}$$

where n is the number of individual birds, and $\overline{\sigma^\circ_B}$ is the average radar cross section (in m^2) of an individual bird.

The average radar cross section of an individual bird is summarized in Table A.6.1.* Radar cross section at intermediate frequencies is to be determined by linear interpolation of radar cross section (dB) against log f. It is assumed that light migratory and non-migratory birds have equivalent radar cross section.

Table A.6.1 Average Radar Cross Section of Individual Birds

Frequency (GHz)	Bird Radar Cross Section (dBm^2) Heavy Migratory (25 gm)	(120 gm)	Light, Non-Migratory (1,000 gm)
0.5	-46	-33	-15
1.2	-34	-23	-22
3.0	-29	-26	-23
5.0	-31	-28	-25
10.0	-33	-31	-27
15.0	-36	-33	-30
30.0	-39	-36	-33
60.0	-42	-38	-36

Assumed bird size for heavy migratory types is between 25 and 120 gm, depending on species. Light migratory types are assumed to weigh 1,000 gm.

A.6.4   Spatial Distribution of Radar Cross Section*

The spatial distribution of radar cross section from cell to cell varies in proportion to the number (n) of individual birds within the cell, which is assumed to follow a Poisson process:

$$p(n) = \frac{\mu^n e^{-\mu}}{n!}$$

where μ is the mean value of n over a widespread area; it is calculated by:

$$\mu = d_i A_c$$

where A_c is the clutter cell area (m^2), and d_i is the average density of birds (m^{-2}), defined below. For $\mu > 9$, the Poisson variate may be approximated by the normal variate with mean μ, and standard deviation $\sqrt{\mu}$.

The average density of birds is assumed to be 1,000 per km^2 (3437 per nmi^2) for heavy migration, 1 per km^2 (3.4 per nmi^2) for light migration, 0.1 per km^2 (0.34 per nm^2) for non-migratory types.

A.6.5 Temporal Distribution of Radar Cross Section

The radar cross section may be assumed to vary with time as given by the exponential density function defined in Section A.2.5.*

A.6.6 Velocity Distribution*

The distribution of migrating bird velocities is assumed to follow the Gaussian distribution specified in Section A.2.6 with $\sigma_v = 2.5$ m/s (4.9 knots). For migrating birds, the mean velocity is assumed to be a function of Azimuth: $V = V_{max} \cos\theta$, where θ is the angle between the radar-look azimuth and the mean migration direction. V_{max} may be 15 m/s (29.1 knots) greater than the mean wind speed, which is as specified in Section A.2.6.2. For non-migratory birds, the flight velocity is assumed to be 10 m/s (19.4 knots) with respect to the mean wind velocity, and having a uniformly random distribution of directions with respect to the mean wind vector.

A.6.7 Frequency Correlation

When a single bird is in the resolution cell, the back-scattered power is independent of frequency shift. When two or more birds are within a single resolution cell, back-scattered power is assumed to change with frequency agility in accordance with a many-scatterer model as described in Section A.2.7. The mean power in a cell and its statistical distribution remains unaffected by frequency agility.

A.6.8 Commentary and Cautionary Notes

A.6.8.1 Bird Type

Radar cross section values listed in Table A.6.1 approximately correspond to the data of Pollon (1971), in which the heavy migration type corresponds to a bird weighing 25 gm (e.g., sparrow) to 120 gm (e.g., grackle). Larger individual birds (e.g., geese), will have a larger radar cross section, especially at the low radar frequencies.

A.6.8.2 Bird Density

Densities of birds in flight can vary greatly with respect to the time of day, the season, and the geographic location. Bird densities under specific conditions can exceed the values listed in Section A.6.4. At low altitudes (< 200 m), densities of non-migrating birds can increase significantly above the cited values. Bird densities are cited as an area proportional metric, which is applicable if the altitude extent of the bird layer is within the illuminated height of the radar cell.

A.6.8.3 Spatial Distribution

The Poisson distribution cited in Section A.6.4 is based on the assumption that birds are located in space with uniform probability. Spatial distribution in fact may be highly non-uniform.

A.6.8.4 Temporal Distribution of Radar Cross Section

Radar cross section values listed in Table A.6.1 approximately correspond to the data of Pollon (1971), in which the heavy migration type corresponds to a bird weighing 25 gm (e.g., sparrow) to 120 gm (e.g., grackle), and the light migration type corresponds to a bird weighing 1,000 gm (e.g., duck). The radar cross section of a single bird will vary with its aspect, and will also vary temporally in synchrony with its wing beat. The exponential distribution cited in Section A.6.5 is a simplification of the radar cross section distribution of a single bird, but converges to theoretical expectations when several birds are in a resolution cell.

A.6.8.5 Velocity Distribution

The cited velocity data are taken as example values. Absolute velocity and its distribution may be greater under specific conditions.

A.7.0 INSECTS

A.7.1 Spatial Extent*

Insects are assumed to be present over land to a maximum range limited only by propagation visibility. Insects may be present over the sea to a range of 20 km (10.8 nmi) from the coast. Altitude distribution may be of two types: surface layer and elevated layer. The surface layer can exist over land; the elevated layer can exist over land or sea. The altitude extent of the surface layer is assumed to be 1 km (3280 ft); the thickness of the elevated layer is 100 m (328 ft). The elevated layer may be centered at any altitude, from the surface to 3 km (9.8 kft).

A.7.2 Clutter Return Power

The clutter return power from a single radar resolution cell is directly proportional to the radar cross section of the insects contained within the cell. The radar cross section is taken to be the product of the volume of the resolution cell (V_c) and the normalized radar cross section (σ°) of the insect swarm, i.e., the radar cross section area per unit volume (m^2/m^3). The volume of the resolution cell is determined by the beam width and the range/Doppler resolution capability of the radar. In addition, it may be limited by the vertical extent of the insect layer.

A.7.3 Normalized Radar Cross Section*

The median value of the normalized radar cross section (σ°_{50}) may be related to radar frequency (f) by:

$$\sigma^\circ_{50} = \begin{cases} K\left(f/f_o\right)^4, & f < 3.3 \text{ GHz} \\ K\left(f/f_o\right)^3, & f \geq 3.3 \text{ GHz} \end{cases}$$

where $f_o = 3.3$ Ghz. When σ°_{50} is expressed in m^2/m^3, the constant K equals 10^{-11} for a surface layer, and equals 10^{-9} for an elevated layer. Table A.7.1 summarizes the median normalized radar cross section of insect swarms at several radar frequencies.

Table A.7.1 Normalized Radar Cross Section of Insect Swarms

Frequency (Ghz)	Normalized Radar Cross Section (dBm^2/m^3)	
	Surface Layer	Elevated Layer
0.5	-142.8	-122.8
1.25	-126.9	-106.9
3.3	-110.0	-90.0
5.6	-103.1	-83.1
9.3	-96.5	-76.5
17.0	-88.6	-68.6
35.0	-79.2	-59.2
70.0	-70.2	-50.2

A.7.4   Spatial Distribution of Radar Cross Section*

The normalized radar cross section of an insect swarm is assumed to remain constant over an area having length and breadth equal to 500 m (0.27 nmi). The variation from one resolution cell to another may be expressed by a log-normal distribution with a median value as expressed in Section A.7.3, and a standard deviation of 5 dB with respect to the median.

Example: Assume surface layer insects and f = 3.3 Ghz,

$$\sigma^{\circ}_{50} = -110 \text{ dBm}^2/\text{m}^3$$

$$\sigma^{\circ}_{84} = -105 \text{ dBm}^2/\text{m}^3$$

A.7.5   Temporal Distribution of Radar Cross Section

In a fixed resolution cell, the radar cross section is assumed to vary with time as described in Section A.2.5, but where the variation period of the median value of the normalized radar cross section is 15 s .

A.7.6   Velocity Distribution

Insect velocity will correspond to that of the local winds. Accordingly, the mean and standard deviation of the velocity spectrum may be determined as stated in Section A.2.6,* except that the term σ_f should be ignored.

A.7.7   Frequency Correlation

Frequency correlation is defined in Section A.2.7.

A.7.8   Commentary and Cautionary Notes

A.7.8.1   Episodic Nature of Insect Clutter

Episodes of insect clutter can vary greatly with respect to the time of day, the season, and the geographic location. The specification in Section A.7.0 applies to a relatively heavy concentration, but not the most severe condition that may be encountered. Available information is not adequate to assign probabilities of occurrence to the stated conditions.

A.7.8.2   Spatial Extent

The area distribution of insects is difficult to specify. Local wind patterns can concentrate insects, and carry them dozens of miles out to sea under some conditions. The altitude distribution cited in Section A.7.1 has been adapted from a few published examples.

A.7.8.3   Median Normalized Radar Cross Section

The median normalized radar cross section corresponding to $K = 10^{-11}$ (Section A.7.3) is thought to represent a relatively heavy concentration of insects. The specified spatial variation (Section A.7.4) will result in specific areas having both greater and lesser radar cross section values. Values have been reported for relatively extreme insect concentrations that exceed the cited values by orders of magnitude. The specification of $K = 10^{-9}$ for layered insects has been selected to account for the increased density of insects when they are concentrated in layers.

The frequency power laws, f^3 and f^4, have been indicated by Hardy and Katz (1969) to apply to the range 0.4 to 10 Ghz. This document extends that range to 70 Ghz. The frequency dependence above 10 Ghz is uncertain because insect-size objects begin to enter the radar cross section resonance region, and the frequency dependence will be highly dependent on the size, shape, and orientation of the scatterers. The extension to mm wave-lengths is especially uncertain.

A.7.9.4   Spatial Distribution

It is reasonable to expect a lumpy distribution of biological objects such as insects. However, it is difficult to determine a spatial model from available information. Lacking specific information, a spatial distribution has been assumed.

A.7.9.5   Mean Velocity

The surface wind velocity referenced in Section A.7.6 is a relatively large value. Over the ocean it corresponds to Sea State 5. Surface winds corresponding to other sea states may be approximately determined as described in Section A.4.3.3.

A.8.0 BACKGROUND REFERENCES

The following references provide a sample of background material applicable to the clutter models discussed in this report

Barton, D.K. (1975). *Radars Vol. 5 - Radar Clutter*. Artech House Inc., Dedham, Mass.

Barton, D.K. (1985). "Land Clutter Models for Radar Design and Analysis," *Proc. IEEE*, 73 (2):198-204.

Barton, D.K. (1985). "Land Clutter Models for Radar Design and Analysis." *Proc. IEEE*, 73(2):198-204.

Barton, D.K. (1988). *Modern Radar System Analysis*, Artech House, Inc., Norwood, MA.

Battan, L.J. (1973). *Radar Observations of the Atmosphere*. The University of Chicago Press, Chicago.

Billingsley, J.B. (1993). "Ground Clutter Measurements for Surface-Sited Radar." Technical Report 786, Rev. 1, MIT Lincoln Lab.

Blake, L.V., (1986). *Radar Range Performance Analysis*. Artech House Inc., Norwood, MA.

Boothe, R.R., (1969). "The Weibull Distribution Applied to the Ground Clutter Backscatter Coefficient." Report RE-TR1-69-115, US Army Command, Redstone Arsenal, AL, AD691109.

CCIR (1986). "Recommendations and Reports of the CCIR," 1986 Volume V, "Propagation in Non-Ionized Media." International Telecommunication Union, Geneva.

CCIR, (1986). Recommendations and Reports of the CCIR, 1986 - Volume V, "Propagation in Non-Ionized Media." International Radio Consultative Committee (CCIR). Geneva.

Dyer, F.B., Currie, N.C., and Applegate, M.S., (1997). "Radar Backscatter from Land, Sea, Rain, and Snow at Millimeter Wavelengths." *Proc. International Conference, Radar-77*, London.

Fletcher, C, (1983). "Clutter Subroutine." Technology Service Corp., Silver Spring, MD, Memorandum TSC-84-01.

Gossard, E.E., and Strauch, R.G., (1983). *Radar Observation of Clear Air and Clouds*. Elsevier, Amsterdam.

Hardy, K.B., and Katz, I., (1969). "Probing the Clear Atmosphere with High-Power, High Resolution Radars." *Proc. IEEE*, 87: 468-479.

Horst, M.M. F. B. Dryer, and M. T. Tuley (1978). "Radar Sea Clutter Model." *Int. Conf. on Antennas and Prop.*, IEE Conf. Pub. 169, Pt 2.

Katzin, M. (1957). "On the Mechanisms of Radar Sea Clutter." *Proc. IRE*, 45(1):44-54.

Kinsman, B., (1968). *Wind Waves*, Dover Publications Inc., New York.

Konrad, T.G., Hicks, J.J., and Dobson, E.B., (1968). "Radar Characteristics of Birds in Flight." *Science*, 159:274-280.

Lin, C.C. (1996). "Initial Radar Clutter Modeling for Man-Made Seaborne Objects." JHU/APL, A3B-97-2-001, Jan. 7, 1996.

Long, M.W. (1983). *Radar Reflectivity of Land and Sea*, Artech House, Inc., Dedham, MA.

Long, M.W. (1983). *Radar Reflectivity of the Sea*, Artech House, Dedham, MA.

M.I.T. Lincoln Laboratory (1984). "Clutter and Jamming Models of Surveillance Subsystems." Section C-1 to C-6 (Unclassified Sections). Contributions to ATRS Working Group.

Morchin W.C. (1993). *Radar Engineer's Sourcebook*. Artech House Inc., Norwood, MA.

Nathanson, F.E. and J. P. Reilly, (1968). "Radar Precipitation Echoes." *IEEE Trans. Aerospace and Elec. Sys.*, AES-4, (4): 504-514.

Nathanson, F.E. and J.P. Reilly (eds), (1969). "Radar Clutter Effects." Johns Hopkins University/Applied Physics Laboratory Report TG-842-1, AD 375 009L.

Nathanson, F.E. J.P.Reilly, and M. Cohen (1991). *Radar Design Principles, 2nd Edition*, McGraw-Hill Inc., New York.

Nathonson, F.E., Reilly, J.P., and Cohen, M.N., (1991). *Radar Design Principles*. (Second Edition). McGraw-Hill Book, Co., New York.

Olin, I.D. (1982). "Amplitude and Temporal Statistics of Sea Spike Clutter." *International Conference, Radar-82*, London.

Pollon, G.E. (1971). "Distribution of Radar Angels." *IEEE Trans. Aero. Elect. Sys.*, AES-8 (6):721-727.

Reilly, J.P. (1988). "Clutter Models for Shipboard Radar Applications: 0.5 to 70 GHz." JHU/APL, F2A-88-0-307R2, Oct. 1, 1988.

Reilly, J.P. C. C. Lin (1994). "A Radar Clutter Model and its Verification." *Proc. 1994 International Geoscience and Remote Sensing Symposium*, Paper 940159, Bermerhaven, Germany.

Reilly, J.P. C. C. Lin, (1995). "Radar Terrain Effects Modeling for Shipboard Radar Applications." JHU/APL, FS-95-060.

Riley, J.R. (1985). "Radar Cross Section of Insects." *Proc. IEEE*, 72(2):228-232.

Rivers, W. (1981). "Doppler Spectra of Radar Clutter," Technology Service Corp., Silver Spring, MD. Report No. TSC-W25-227, Nov. 30, 1981 (D-A111306).

Rivers, W., F.E. Nathanson, and L. Blake, (1977). "Shipboard Surveillance Radar Environment Models." Technology Service Corp. Report No. TSC-W-25-118, April 25, 1977.

Rogers, R. R. (1976). "Statistical Rainstorm Models." *IEEE Trans. Ant. Prop.*, (July):547-566.

Sittrop, H. (1977). "On the Sea Clutter Dependency on Windspeed." *Proc. International Conference, Radar-77,* London.

Skolnik, M.I. (1990). *Radar Handbook (Second Edition)*. McGraw-Hill, Inc., New York.

Trebits, R.N., M.M Horst, M.W. Long, N.C. Currie, and J.W. Peifer, (1978). "Millimeter Radar Sea Return Study." Georgia Institute of Technology, Report No. GIT/EES A-2012 ITR.

U.S. Air Force (1961). *Handbook of Geophysics*. The MacMillian Co., New York.

Vaughn, C.R. (1985). "Birds and Insects as Radar Targets: A Review." *Proce. IEEE,* 73(2):205-226.

Ward, K.D. (1982). "A Radar Sea Clutter Model and Its Application to Performance Assessment." *Proc. International Conference, Radar-82,* London.

A1A97U-070

SECTION B

BISTATIC SCATTERING MODELS

Prepared by:

R.L. McDonald
The Johns Hopkins University
Applied Physics Laboratory
Johns Hopkins Road
Laurel, MD 20723-6099

Table of Contents

A1A97U-070

B.1.0 PURPOSE

The purpose of this section is to define bistatic scattering models for distributed surfaces. Section B.2.0 addresses bistatic backscatter from sea and land, while Section B.3.0 pertains to forward scatter. These models are based on the best information available, but in many cases information is incomplete. Engineering judgment has been used in the interest of completeness with anticipation that models will be refined as new information becomes available. Each section is accompanied by a subsection entitled "Commentary and Cautionary Notes" intended to emphasize major areas of uncertainty, qualification, and simplification.

B.2.0 BACKSCATTER

Bistatic backscatter is applicable to interceptors which employ semiactive guidance based on target illumination from a remote platform. The platform may be airborne or surface-based.

B.2.1 Sea Return

This section presents a method for calculating the bistatic sea return. It is closely derived from Section A.4.0 which addresses monostatic sea clutter.

B.2.1.1 Spatial Extent

The bistatic sea return is assumed to exist at all azimuths up to the nearer of the 4/3 earth radar horizons associated with the transmitter and receiver. During ducting conditions, the sea return is assumed to be visible to ranges strongly dependent on the refractive properties of the propagation duct.

B.2.1.2 Clutter Return Power

The clutter return power from a single radar resolution cell is directly proportional to the bistatic radar cross section of the sea surface contained within the cell. The bistatic radar cross section is taken to be the product of the surface area (A_c) corresponding to the resolution cell and the normalized bistatic radar cross section (σ°_B) of the surface, i.e.,

B-1

the bistatic radar cross section per unit of surface area (m^2/m^2).

The resolution cell area is the surface area contained within iso-range and iso-Doppler contours associated with the range gate and Doppler resolution bandwidth of the system. In addition, the one-way antenna pattern weightings of the transmit and receive beams must be used in place of the two-way beam shape factor used in monostatic applications. In cases where the area resolution cell is sufficiently large that the average back-scattered power varies spatially across the cell, the cell must be subdivided and contributions non-coherently summed to calculate the total average power.

B.2.1.3 Normalized Radar Cross Section : Standard Atmosphere

The equations presented in this section apply to "standard atmosphere" propagation conditions. Grazing angles are to be calculated assuming a 4/3 round-earth radius.

The wide-area mean value of the normalized bistatic radar cross section for X-band, vertically polarized, cross-wind transmissions at large (> 1 degree) grazing angles is given by

$$\overline{\sigma^{\circ}_B} = \gamma \, \sin(\psi_i)\sin(\psi_r)$$

where ψ_i, ψ_r are the grazing angles of incidence and reflection, and
γ is a sea-state dependent parameter.

For Sea State 3, γ is 0.05 (-13 dB). γ varies linearly with sea state at 4.5 dB/sea state. At small transmit grazing angles, the normalized bistatic radar cross section is independent of the receiver grazing angle and equal to the monostatic value associated with the incident grazing angle alone. The monostatic value, as well as adjustments to the bistatic value, above, for frequency, polarization, and wind direction are to be calculated as defined in Section A.4.3 using the incident grazing angle. The monostatic multipath interference adjustment factor, G_a, should be replaced by

$$G_a = \frac{a_i^2}{(1 + a_i^2)} \times \frac{a_r^2}{(1 + a_r^2)}$$

where a_i and a_r are to be calculated using the incident and reflected grazing angles

respectively. The normalized bistatic radar cross section is to be taken as the larger of the bistatic and monostatic values.

B.2.1.4 Normalized Radar Cross Section : Ducting Conditions

Calculation of sea return levels under surface-based ducting conditions will be accomplished in a manner similar to that defined for monostatic sea clutter in Section A.4.4. Refractive effects can be significant when the transmit grazing angle is less than 1.5 degrees. Typically, the receive grazing angle is sufficiently large that propagation effects do not apply to the receive path.

In calculating the bistatic return, the "standard atmosphere" propagation factor is to be removed from the monostatic value, the grazing angles are to be calculated using an optical ray trace method, and the one-way propagation factors associated with the transmitter and receiver (if necessary) are to be applied. The propagation factors are to be calculated using a high-fidelity propagation model (see Section C.7.0).

B.2.1.5 Statistical Distribution of Radar Cross Section

The statistical variation of the normalized bistatic radar cross section is described here as a compound distribution, in which the value for a fixed resolution cell varies with time in accordance with an exponential distribution whose mean changes from cell to cell according to the Weibull distribution. In cases where the bistatic geometry changes or the position of the resolution cell on the surface moves between looks, such as when tracking a moving target, temporal correlation of the clutter return is not of interest. In such cases the compound distribution can be approximated as a Weibull distribution with a constant wide-area mean from cell to cell and a larger slope parameter (See Section A.4.6.4). Discrete clutter is treated as an additional feature.

B.2.1.6 Spatial Distribution

For high resolution systems at low grazing angles, the mean value of the normalized bistatic radar cross section is assumed to vary from one resolution cell to another in accordance with the Weibull density function (Section A.4.6) with a slope parameter as defined in Section A.4.6.1. For large resolution cells and/or higher grazing angles, the Weibull slope parameter approaches unity. In these cases the Weibull density function reduces to the exponential density function,

$$p(\sigma^{\circ}_B) = \frac{1}{\overline{\sigma^{\circ}_B}} \exp\left[-\frac{\sigma^{\circ}_B}{\overline{\sigma^{\circ}_B}}\right]$$

where $\overline{\sigma^{\circ}_B}$ is the wide-area mean value of the normalized bistatic radar cross section as defined above. In cases where temporal correlation is not of interest, the Weibull slope parameter associated with the compound spatial distribution defined in Section A.4.6.4 can be used instead of the temporal distribution model defined below.

B.2.1.7 Temporal Distribution

For a fixed radar resolution cell, the back-scattered power is assumed to fluctuate over short time intervals ($t\ll 1s$) in accordance with the exponential density function specified in Section A.2.5 and with a fluctuation spectrum derived from the velocity distribution specified in Section A.4.9. For long-term observations the mean power in a fixed resolution cell is assumed to vary slowly in accordance with the spatial distribution specified above. This slow fluctuation will vary on a time scale consistent with the period of the significant sea waves (about 1 to 10 s over the range of sea states from 1 to 6). When the transmitter and/or receiver are moving, the fluctuation spectrum due to sea wave motion will typically be negligible compared with Doppler spreading.

B.2.1.8 Discrete Sea Clutter

Discrete sea clutter sources, including man-made objects and sea spikes, are to be modeled as point reflectors with the characteristics defined in Section A.4.8.

B.2.1.9 Commentary and Cautionary Notes

The bistatic model defined in B.2.1.3 is based on limited measurements made for the Navy Mountain Top Program. Measurements made at low transmit grazing angles (<< 1 deg) appeared to be independent of receive grazing angle, while measurements at high transmit grazing angles (> 1 deg) showed a first-order dependence on receive grazing angle (5-45 degrees). Transmit grazing angles were limited during the test program to 10 degrees, maximum. Since the bistatic model is largely derived from the monostatic model specified in Section A.4.0, the commentary and cautionary notes expressed in Section A.4.11 concerning the monostatic model apply to the bistatic case, as well.

B.2.2   Land Return

This section presents the method for calculating the bistatic land return. It is closely derived from Section A.5.0 which addresses monostatic land clutter. Typically, the receiver views land clutter at larger grazing angles than does the transmitter. The characteristics of the bistatic land return are assumed to be independent of the receiver grazing angle and identical to those of monostatic land clutter at the grazing angle associated with the transmitter, i.e., land features reflect isotropically.

B.2.2.1   Spatial Extent

The spatial extent of the bistatic land return will be as specified in Section A.5.1 for high-relief and low-relief environments. The land return will be visible within a band that depends on terrain relief, transmitter location, and propagation conditions.

B.2.2.2   Clutter Return Power

The clutter return power from a single radar resolution cell is directly proportional to the bistatic radar cross section of the sea surface contained within the cell. The bistatic radar cross section is taken to be the product of the surface area (A_c) corresponding to the resolution cell and the normalized bistatic radar cross section (σ°_B) of the surface, i.e., the bistatic radar cross section per unit of surface area (m^2/m^2).

The resolution cell area is the surface area contained within iso-range and iso-Doppler contours associated with the range gate and Doppler resolution bandwidth of the system. In addition, the one-way antenna pattern weightings of the transmit and receive beams must be used in place of the two-way beam shape factor used in monostatic applications. In cases where the area resolution cell is sufficiently large that the average back-scattered power varies spatially across the cell, the cell must be subdivided and contributions non-coherently summed to calculate the total average power.

B.2.2.3   Normalized Radar Cross Section

The mean value of the normalized bistatic radar cross section is taken to be independent of the receiver grazing angle and equal to the monostatic value associated with the incident grazing angle alone. The monostatic value is to be calculated as specified in Section A.5.3.

B.2.2.4 Inclusion of Propagation Factor

Calculations of the bistatic land return will include the one-way propagation factor, F^2, associated with the transmit path (See Section A.5.3.3). The propagation factor associated with the receive path is assumed to be unity.

B.2.2.5 Elevation Coverage

Under standard atmosphere conditions, the maximum elevation angle required to illuminate the terrain can be calculated based on the peak terrain height specified in Section A.5.1, assuming a 4/3 earth radius. Under ducting conditions, the maximum elevation angle supporting propagation within the duct may be assumed to be less than one degree. For propagation outside the duct, a standard atmosphere calculation may be used to determine elevation.

B.2.2.6 Temporal Distribution

For a fixed resolution cell, the back-scattered power is assumed to fluctuate in accordance with the exponential density function specified in Section A.2.5 and with a fluctuation spectrum derived from the velocity distribution specified in Section A.5.8. When the transmitter and/or receiver are moving, the fluctuation spectrum due to wind-blown vegetation will typically be negligible compared with Doppler spreading.

B.2.2.7 Discrete Clutter

Discrete clutter sources are to be modeled as point reflectors with the characteristics defined in Section A.5.7.

B.2.2.8 Commentary and Cautionary Notes

The assumed independence of normalized bistatic radar cross section on the receive grazing angle is speculative. For the airborne transmit platform, the bistatic angle may be small resulting in a near monostatic condition. No bistatic measurement data exist for land- or sea-based illuminators. Since the bistatic model is largely derived from the monostatic model specified in Section A.5.0, the commentary and cautionary notes expressed in Section A.5.10 concerning the monostatic model apply to the bistatic case, as well.

A1A97U-070

B.3.0 FORWARD SCATTER

Specular forward scatter from the surface of the earth can result in coherent multipath interference producing signal fluctuations in surveillance, communications, and interceptor guidance systems. Diffuse forward scatter can produce a non-coherent return which limits detection and tracking of low-flying targets. The target may attempt to exploit this phenomenon with appropriate use of ECM (hot clutter). The magnitude and spectral characteristics of forward scatter vary with the apparent surface roughness, which is wavelength and grazing-angle dependent.

This section addresses forward scatter assuming "standard atmosphere" conditions. The intent of this model is to provide a means of calculating the signal parameters of multipath interference in cases where discrimination between the desired direct-path and undesired indirect-path returns may be possible. In these cases the indirect-path grazing angles are typically sufficiently large for "standard atmosphere" propagation to be assumed. For calculating propagation factors under ducting conditions, see Section C.7.0.

B.3.1 Sea Bounce

B.3.1.1 Specular Scatter

Specular reflection occurs in a small region on the surface around the specular point, at which the incidence and reflection angles are equal. These angles are to be calculated assuming a 4/3 round-earth radius.

The amplitude of the specularly reflected signal is determined by the range ($1/R^2$) loss associated with the total path length (from the source to the specular point to the receiver) and the magnitude of the coherent reflection coefficient of the surface. For the case in which a target-reflected signal is the source and a multi-reflector target model is not employed, the direct-path and indirect-path signal amplitudes are assumed to fluctuate independently, but with the same statistics. The phase of the reflected signal relative to that at the source is determined by the total path length, the wave number ($2\pi/\lambda$), and the phase contribution of the coherent reflection coefficient.

The coherent reflection coefficient, ρ_c, is given by

$$\rho_c = \rho_s \rho_o D$$

where ρ_s is the rough-surface specular reflection coefficient,

ρ_o is the Fresnel reflection coefficient for sea water, and

D is the divergence factor.

Details for calculating the coherent reflection coefficient are given in Section C.

B.3.1.2 Diffuse Scatter

Diffuse scattering occurs over a region of the surface about the specular point. The primary contribution is from the reflection region known as the "glistening surface", which is comprised of individual, large-scale wave facets, each properly oriented to produce a specular reflection in the desired direction. Wide-angle scattering from small-scale roughness also occurs.

B.3.1.2.1 Spatial Extent

The "glistening surface" return is the non-coherent summation of the specular reflections from the individual wave facets on the glistening surface. The wave-facet slope distribution is assumed to be isotropically Gaussian with a zero mean and a standard deviation equal to the RMS wave slope, $\tan(\beta_o)$, specified for 10 GHz in Table B.1.

Table B.1
Sea Wave Parameters

Sea State	0	0+	1	2	3	4	5	6
Wind (kts) (m/s)	0-1 0-0.5	1-3 0.5-2	4-6 2-3	7-10 3-5.5	11-16 5.5-8	17-21 8-11	22-27 11-14	28-47 14-24
Wave Height Crest/Trough (m)	0-0.001	0.001-0.04	0.04-0.1	0.1-0.5	0.5-1.25	1.25-2.5	2.5-4.0	4.0-6.0
RMS Wave Slope (10 GHz)	0.05	0.09	0.12	0.14	0.15	0.16	0.18	0.22

At frequencies other than 10 GHz the RMS wave slope is given by

$$\tan(\beta_o) = \sqrt{0.6 + 0.4\,(f\,/\,f_o)}\ \tan(\beta_o)_{10\,GHz}, \quad f < 35\,GHz$$
$$= \sqrt{2}\ \tan(\beta_o)_{10\,GHz} \qquad\qquad , \quad f \geq 35\,GHz$$

where f is the frequency in GHz, f_o is equal to 10 GHz, and $\tan(\beta_o)_{10\,GHz}$ is the RMS wave slope at 10 GHz specified in Table B.1.

The spatial extent of the glistening surface varies with the location of the signal source and the receiver, but is assumed to include, at a minimum, all points at which the required wave-facet slope, $\tan(\beta)$, as specified in Section B.3.1.2.3, is less than three times the RMS wave slope.

B.3.1.2.2 Forward Scattered Power

The forward scattered power for a single radar resolution cell is directly proportional to the bistatic radar cross section of the sea surface contained within the cell. The bistatic radar cross section is taken to be the product of the surface area (A_c) corresponding to the resolution cell and the normalized bistatic radar cross section (σ°_B) of the surface, i.e., the bistatic radar cross section per unit of surface area (m^2/m^2).

The resolution cell area is the surface area contained within iso-range and iso-Doppler contours associated with the range gate and Doppler resolution bandwidth of the system. In addition, the one-way antenna pattern weightings of the transmit and receive beams must be used in place of the two-way beam shape factor used in monostatic applications. In cases where the area resolution cell is sufficiently large that the average forward-scattered power varies spatially across the cell, the cell must be subdivided and contributions non-coherently summed to calculate the total average power.

B.3.1.2.3 Normalized Radar Cross Section

The mean value of the normalized bistatic radar cross section of the glistening surface is the product of two terms, one accounting for the wave-slope dependence and one characterizing the reflectivity of individual wave facets,

$$\overline{\sigma^\circ_B} = f(\beta) \times |\rho(\alpha)|^2$$

$$f(\beta) = \frac{\exp[-\tan^2(\beta)/\tan^2(\beta_o)]}{\tan^2(\beta_o)\cos^4(\beta)}$$

where $\tan(\beta)$ is the wave slope required to produce specular reflection in the desired direction,

$\tan(\beta_o)$ is the RMS wave slope specified in Section B.3.1.2.1,

$\rho(\alpha)$ is the complex specular reflection coefficient including polarization mismatch effects, and

α is the specular-plane incidence angle.

The angle β is the angle between the bisector of the incident and reflected rays and the surface normal,

$$\cos(\beta) = \frac{\sin(\psi_i) + \sin(\psi_r)}{2\cos(\alpha)}$$

The angle α is the angle between the bisector and either the incident or reflected ray,

$$\cos(\alpha) = \frac{1}{\sqrt{2}}\sqrt{1 - \cos(\psi_i)\cos(\psi_r)\cos(\varphi) + \sin(\psi_i)\sin(\psi_r)}$$

where ψ_i, ψ_r are the grazing angles of incidence and reflection, respectively, at the surface, and

φ is the azimuth angle of reflection ($\varphi = 0$ corresponds to in-plane forward scatter).

The reflectivity of a wave facet is given by

$$\rho_{VV} = \frac{a_2 a_3 \rho_V(\alpha) + \cos(\psi_i)\cos(\psi_r)\sin^2(\varphi)\rho_H(\alpha)}{\sin^2(2\alpha)}$$

$$\rho_{HV} = \frac{a_3 \cos(\psi_i)\sin(\varphi)\rho_V(\alpha) - a_2 \cos(\psi_r)\sin(\varphi)\rho_H(\alpha)}{\sin^2(2\alpha)}$$

$$\rho_{VH} = \frac{a_2 \cos(\psi_r)\sin(\varphi)\rho_V(\alpha) - a_3 \cos(\psi_i)\sin(\varphi)\rho_H(\alpha)}{\sin^2(2\alpha)}$$

$$\rho_{HH} = \frac{\cos(\psi_i)\cos(\psi_r)\sin^2(\varphi)\rho_V(\alpha) + a_2 a_3 \rho_H(\alpha)}{\sin^2(2\alpha)}$$

where the first subscript above is the polarization of the scattered signal, the second subscript is the polarization of the incident signal, and ρ_V, ρ_H are the smooth-surface Fresnel reflection coefficients defined in Section C. The geometrical parameters, a_2 and a_3, are given by

$$a_2 = \sin(\psi_i)\cos(\psi_r) + \cos(\psi_i)\sin(\psi_r)\cos(\varphi)$$

$$a_3 = \cos(\psi_i)\sin(\psi_r) + \sin(\psi_i)\cos(\psi_r)\cos(\varphi)$$

In addition to the forward reflection lobe caused by scattering from the glistening surface, low-level diffuse scattering occurs at wide angles as a result of small capillary waves. The normalized bistatic radar cross section model specified for backscatter in Section B.2.1.3 will be used to calculate the wide-angle scattering contribution. The mean value of the normalized bistatic radar cross section is the sum of the contributions from the glistening surface and wide-angle scattering.

B.3.1.2.4 Spatial Distribution

The spatial distribution of the mean value of normalized bistatic radar cross section from cell to cell is strictly determined by geometry as specified in Section B.3.1.2.3. The spatial distribution of the instantaneous value varies in accordance with an exponential density function, consistent with the temporal distribution specified in Section B.3.1.2.5.

B.3.1.2.5 Temporal Distribution

The diffusely scattered signal power in each resolution cell will vary with time in accordance with the exponential density function (Rayleigh fluctuation) specified in Section A.2.5 and with a fluctuation spectrum derived from the velocity distribution specified in Section A.4.9. When the signal source and/or receiver are moving, the fluctuation spectrum due to sea wave motion will typically be negligible compared with Doppler spreading.

B.3.1.2.6 Commentary and Cautionary Notes

The diffuse forward reflection lobe is modeled in accordance with the theory for noncoherent scattering from a very rough surface discussed in section 9.1.3.5 of Reference (1). The theory strictly applies only when the surface roughness is sufficient to preclude significant specular scattering. In addition, the theory requires that (1) the radius of curvature of surface irregularities is much greater than the wavelength, (2) surface roughness is isotropic in both dimensions with a Gaussian surface-height probability density function, (3) the correlation length of the surface roughness is much less than the dimensions of the area resolution cell, and (4) multiple scattering and shadowing effects are neglected. One application of the model for target image multipath is described in Reference (2). Model validation by means of comparison with test data is limited. Appropriate consideration should be exercised in the use of this model.

The sea wave parameters defined in Table B.1 are taken from Reference (3) with appropriate modifications to reflect the sea state definition endorsed by the World

B-11

Meteorological Organization, which appears in Reference (4). The frequency dependence of the wave slope is based on Reference (5).

B.3.2 Terrain Bounce

B.3.2.1 Specular Scatter

Specular reflection occurs in a small region on the surface around the specular point, at which the incidence and reflection angles are equal. These angles are to be calculated assuming a 4/3 round-earth radius.

Except at low frequencies, the coherent reflection from terrain is typically negligible due to the roughness of the surface. Characteristics of the coherent specularly reflected signal will be calculated as specified in Section B.3.1.1 with details provided in Section C.

B.3.2.2 Diffuse Scatter

Diffuse scattering occurs over a region of the surface about the specular point. The primary contribution is from the reflection region known as the "glistening surface", which is comprised of individual, large-scale surface facets, each properly oriented to produce a specular reflection in the desired direction. Wide-angle scattering from small-scale roughness also occurs.

B.3.2.2.1 Spatial Extent

The "glistening surface" return is the non-coherent summation of the specular reflections from the individual terrain facets on the glistening surface. The facet slope distribution is assumed to be isotropically Gaussian with a zero mean and a standard deviation equal to the RMS facet slope, $\tan(\beta_o)$. The spatial extent of the glistening surface varies with the location of the signal source and the receiver, but is assumed to include, at a minimum, all points at which the required facet slope, $\tan(\beta)$, specified in Section B.3.1.2.3, is less than the maximum facet slope specified in Section B.3.2.2.3.

B.3.2.2.2 Forward Scattered Power

The forward scattered power for a single radar resolution cell is directly proportional to the bistatic radar cross section of the terrain surface contained within the

cell. The bistatic radar cross section is taken to be the product of the surface area (A_c) corresponding to the resolution cell and the normalized bistatic radar cross section (σ°_B) of the surface, i.e., the bistatic radar cross section per unit of surface area (m^2/m^2).

The resolution cell area is the surface area contained within iso-range and iso-Doppler contours associated with the range gate and Doppler resolution bandwidth of the system. In addition, the one-way antenna pattern weightings of the transmit and receive beams must be used in place of the two-way beam shape factor used in monostatic applications. In cases where the area resolution cell is sufficiently large that the average forward-scattered power varies spatially across the cell, the cell must be subdivided and contributions non-coherently summed to calculate the total average power.

B.3.2.2.3 Normalized Radar Cross Section

Separate diffuse scattering models are specified for the 0.1 -1 GHz and the 1-70 GHz bands. For the 0.1-1 GHz band the maximum facet slope is taken to be 3 times the RMS facet slope. For the 1-70 GHz band the maximum facet slope is taken to be $\tan(\pi/4)$.

B.3.2.2.3.1 Model for the 0.1-1 GHz Frequency Band

Diffuse scattering from the glistening region will be modeled for the 0.1-1 GHz band in accordance with the Beckmann - Spizzichino (exponential) formulation, Reference (6), with wide-angle scattering included based on a bistatic-monostatic equivalence assumption. The corresponding terms are to be summed, so that the larger of the two terms dominates in its respective region,

$$\overline{\sigma^\circ_B} = \cot^2(\beta_o) \exp\left\{-\left[\tan^2(\beta)/\tan^2(\beta_o)\right]\right\} + \gamma \sin(\psi_{equiv}),$$

where the equivalent grazing angle is defined by

$$\sin(\psi_{equiv}) = maximum\ of\ \left\{\ \sin(10^\circ),\quad \sqrt{\sin(\psi_i)\sin(\psi_r)}\ \right\}$$

and ψ_i, ψ_r are the grazing angles of incidence and reflection, respectively. The parameters β_o and γ are specified in Table B.2.

Table B.2 Bistatic Parameters (0.1 - 1 GHz)

Terrain Type	$\tan(\beta_o)$	γ
Urban	0.5	-2.4 dB
High Relief	0.4	-12.4 dB
Low Relief	0.1	-22.4 dB

Note that the value of bistatic scattering for $\psi_i = \psi_r$ and $\varphi = \pi$, which corresponds to monostatic backscatter, reduces to the form in Section A.5.3.1.

B.3.2.2.3.2 Model for the 1-70 GHz Frequency Band

The model for 1-70 GHz includes two independent variables, θ_S and θ_B, which can be computed from the surface-slope angle (β) and the specular incidence angle (α), defined in Section B.3.1.2.3,

$$\theta_S = \sqrt{2(\alpha^2 + \beta^2)}$$

$$\theta_B = 2\,|\beta|, \quad |\beta| < \frac{\pi}{4}$$

$$= \frac{\pi}{2} \quad , \quad |\beta| \geq \frac{\pi}{4}$$

The mean value of the normalized bistatic radar cross section for rural, forested, and urban terrain is given below. Rural and forested terrain may be low or high relief as specified in Section A.5.1.

Rural Terrain

The mean value of the normalized bistatic radar cross section is given by

$$\overline{\sigma^\circ_B} \ (\text{m}^2/\text{m}^2) = \max[\ S_1, S_2\ ]$$

A1A97U-070

$$S_1 = -0.304 \, \theta_B + 0.252 \qquad\qquad , \theta_B \leq 0.75 \text{ radians}$$

$$= -0.015 \, \theta_B + 0.034 \qquad\qquad , \theta_B > 0.75 \text{ radians}$$

$$S_2 = m \, \theta_B + c$$

where

$$m = -0.34 - 2.04 \, \theta_S \qquad\qquad , \theta_S \leq 1.23 \text{ radians}$$

$$= 25.64 - 23.1 \, \theta_S \qquad\qquad , \theta_S > 1.23 \text{ radians}$$

and

$$c = 0.252 + 0.36 \, \theta_S \qquad\qquad , \theta_S \leq 1.23 \text{ radians}$$

$$= -5.68 + 5.17 \, \theta_S \qquad\qquad , \theta_S > 1.23 \text{ radians}$$

Forested Terrain

The mean value of the normalized bistatic radar cross section is given by

$$\overline{\sigma^\circ_B} \, (dB) = -5.73 \, \theta_S - 12.0 \qquad\qquad , \theta_S \leq 1.456 \text{ radians}$$

$$= \max[\, S_1, S_2 \,] \qquad\qquad , \theta_S > 1.456 \text{ radians}$$

where

$$S_1 = -5.73 \, \theta_S - 12.0 \qquad\qquad , \theta_S \leq 1.5708 \text{ radians}$$

$$= -9.23 \, \theta_S - 6.5 \qquad\qquad , \theta_S > 1.5708 \text{ radians}$$

$$S_2 = m \, \theta_B + c$$

and

$$m = -5.729 \qquad\qquad , \theta_S \leq 1.71 \text{ radians}$$

$$= \max [\, 184.7 - 111.4 \, \theta_S , -34.374] \qquad , \theta_S > 1.71 \text{ radians}$$

$$c = -37.5 + 10.3 \, \theta_S \qquad\qquad , \theta_S \leq 1.71 \text{ radians}$$

$$= -82.64 + 36.3 \, \theta_S \qquad\qquad , \theta_S > 1.71 \text{ radians}$$

Urban Terrain

The mean value of the normalized bistatic radar cross section is given by

$$\overline{\sigma^{\circ}_B} \; (m^2/m^2) \; = \; max[\; S_1 \; , \; S_2 \;]$$

$$S_1 \; = \; -1.46 \; \theta_B \; + 1.0 \qquad\qquad , \; \theta_B \; \le \; 0.6161 \; radians$$

$$= \; -0.0081 \; \theta_B \; + 0.032 \qquad , \; \theta_B \; > \; 1.48 \; radians$$

$$= \; -0.0926 \; \theta_B \; + 0.157 \qquad , \; \theta_B \; \le \; 1.48 \; radians \; and$$

$$\theta_B \; > \; 0.6161 \; radians$$

$$S_2 \; = \; m \; \theta_B \; + \; c$$

where

$$m \; = \; -2.06 \; - 4.83 \; \theta_S \qquad\qquad , \; \theta_S \; \le \; 1.235 \; radians$$

$$= \; 48.67 \; - \; 45.9 \; \theta_S \qquad\qquad , \; \theta_S \; > \; 1.235 \; radians$$

and

$$c \; = \; 1.0 \qquad\qquad\qquad\qquad\qquad , \; \theta_S \; \le \; 1.235 \; radians$$

$$= \; -10.27 \; + \; 9.13 \; \theta_S \qquad\qquad , \; \theta_S \; > \; 1.235 \; radians$$

B.3.2.2.4 Spatial Distribution

The spatial distribution of the mean value of normalized bistatic radar cross section from cell to cell is strictly determined by geometry as specified in Section B.3.2.2.3. The spatial distribution of the instantaneous value varies in accordance with the exponential density function consistent with the temporal distribution specified in Section B.3.2.2.5.

B.3.2.2.5 Temporal Distribution

The normalized bistatic radar cross section for a fixed resolution cell will fluctuate with time in accordance with an exponential density function (Rayleigh fluctuation) specified in Section A.2.5. Each resolution cell is modeled as a many-scatterer process with a Gaussian distribution of particle velocities, as specified in Section A.2.6, having a zero mean and a standard deviation of 0.6 m/s for low-relief terrain, 0.3 m/s for high-relief terrain, and 0 m/s for urban terrain. When the signal source and/or receiver are

moving, the fluctuation spectrum due to wind-blown vegetation will typically be negligible compared with Doppler spreading.

B.3.2.2.6 Commentary and Cautionary Notes

The diffuse scattering model for the 0.1-1 GHz band is based on UHF measurements made by MIT/LL. Although the 1 GHz upper limit is somewhat arbitrary, its applicability at higher frequencies is considered questionable based on existing X-band measurements.

The diffuse scattering model for the 1-70 GHz band is based on an empirical X-band model described in Reference (7) for co-planar reflections. The model was extended in Reference (8) to out-of-plane geometries ($\varphi \ll \pi/2$) under the assumption that the surface roughness is isotropic. Application at other frequency bands is speculative based on (1) the assumption that the terrain surface is sufficiently rough that only the reflective properties of the terrain cover are wavelength dependent, and (2) the observation that the frequency dependence of a terrain cover reflectivity consistent with model predictions, i.e., a relatively dry ground or vegetation-covered surface, is not great. Nevertheless, use of the model at other than X-band should be undertaken with caution.

A1A97U-070

B.4.0 REFERENCES

(1) <u>Radar Cross Section Handbook (Volume 2)</u>, by G.T. Ruck, D.E. Barrick, W.D. Stuart, and C.K. Kirchbaum, Plenum Press, New York, 1970.

(2) JHU/APL F1B-2-89U-041, "Multi-Centroid SM-2 Multipath Model," by M. A. Smalley, The Johns Hopkins University Applied Physics Laboratory, Laurel, Maryland, 17 November 1989

(3) JHU/APL F1A(2)89U-003, "Wave Slope Values to be Used in STANDARD Missile Homing Simulations," by M.J. Leumas, 20 January 1989

(4) Designing Ships to the Natural Environment," by S.L. Bales, Association of Scientists and Engineers of the Naval Sea Systems Command, 19th Annual Technical Symposium, April 1982, David Taylor Naval Ship R&D Center, Table 3.

(5) NASA Technical Memorandum 80278, "A Model for the Emissivity of the Ocean's Surface as a Function of Wind Speed," by T.T. Wilheit, Goddard Space Flight Center, Greenbelt, MD, April 1979.

(6) <u>The Scattering of Electromagnetic Waves from Rough Surfaces</u>, by P. Beckmann and A. Spizzichino, Artech House, Inc., Norwood, MA, 1987.

(7) Memorandum No. SIM.1802, "The Bistatic Reflection From Land and Sea of X-Band Radio Waves," by A. R. Domville, G. E. C. (Electronics) Limited, Applied Electronics Laboratories, Stanmore, Middlesex, England, July 1967

(8) JHU/APL F1A-96U-093, "A Forward Scatter Model for STANDARD Missile Overland Engagements," by R. L. McDonald, The Johns Hopkins University Applied Physics Laboratory, Laurel, Maryland, 29 July 1996

A1A97U-070

SECTION C

ATMOSPHERIC PROPAGATION MODELS

Prepared by

G.D. Dockery
The Johns Hopkins University
Applied Physics Laboratory
Johns Hopkins Road
Laurel, MD 20723-6099

and

J. Stapleton
Dahlgren Division
Naval Surface Warfare Center
Dahlgren, VA 22448

Table of Contents

C.1.0 PURPOSE

The propagation effects addressed in this section include atmospheric refraction, diffraction, losses due to precipitation and dust storms, gaseous absorption (oxygen and water vapor), and multipath interference. There is some overlap with Section B, Bistatic Scattering Models, since multipath interference results from forward scatter. Specifically, this section addresses specular, or coherent multipath, while Section B discusses diffuse, or incoherent, multipath.

The importance of the various propagation effects is a strong function of frequency and geometry. In particular, refractive effects are essentially negligible for the situation of an elevated sensor conducting surveillance and/or weapon support for low-altitude targets, such as terrain-following cruise missiles. On the other hand, refractive impacts on participating surface-based systems, e.g., AN/SPY-1 on an AEGIS ship, are substantial. Diffraction effects, particularly as experienced behind terrain features, are important for both geometries, as is gaseous absorption and precipitation attenuation for frequencies above 1 GHz.

The above propagation issues impact the power reaching the target for radar and illumination systems, and the strength of returned clutter power for radar and missile seeker systems. They also impact the tracking performance of surveillance and fire-control radars through changes in SNR and/or signal corruption due to interfering scattering and refractive bending. To accurately account for these effects in system performance evaluations, high fidelity propagation models, or the products thereof, must be incorporated in the forward- and backward-scatter models described elsewhere in this document. The following sections briefly discuss each of the propagation effects and suggest appropriate models for use in system design studies.

C.2.0 ATMOSPHERIC REFRACTION

The two situations requiring consideration of refraction are low-sensor/low-target (LSLT) and high-sensor/high-target (HSHT). LSLT scenarios are impacted by surface-based ducts, evaporation ducts, and subrefraction, while the HSHT cases are sensitive to elevated ducts and elevated subrefractive layers. As a general rule, a propagating ray from a sensor must make an angle of less than 1.5 degrees with a refractive layer in order to be substantially affected, which is why ducting can generally be neglected in low-sensor/high-target (LSHT) and high-sensor/low-target (HSLT) situations. In all cases, a standard atmosphere is the condition assumed in the absence of ducting or subrefraction.

Variations in the refractive index of the atmosphere result from variations in temperature and humidity, and these variations are nominally stratified in horizontal layers. Because the deviations from unity in the refractive index are on the order of 0.01% or less, the quantity "refractivity" is defined for convenience as $N = (n-1) \times 10^6$, where n is the refractive index. It is also convenient to introduce "modified refractivity," which is defined as $M = N + (z/a_e) \times 10^6$, where z is altitude and a_e is the earth's radius. Negative vertical gradients in M correspond to trapping or ducting layers in which rays bend toward the earth's surface. Thus, it is possible to easily identify and define ducting conditions in terms of vertical profiles of M. Substantial deviations from the nominal or quiescent condition are generally limited to the first 5 km (15 kft) of the atmosphere. Above this altitude, the refractivity, N, decreases exponentially with altitude.

The "standard atmosphere" or "4/3-earth" condition is the "nominal" refractive condition referred to above. The corresponding refractivity profile is characterized at low altitudes (below 1.5 km (5 kft)) by a vertical gradient in M of +35.97/kft (+118/km). For higher altitudes, it is necessary to use an exponential function as given in Reference 1,

$$N = 313 \exp(-0.1439\, z) ,$$

where z is the altitude in kilometers. Note that this expression is for "refractivity" not "modified refractivity." The "standard atmosphere" condition serves as the "baseline," and is often considered to be conservative with respect to propagation over the ocean. However, subrefraction is now known to result in much lower energy levels at low altitudes (References 2, 3, and 4), and recent design studies have therefore included subrefractive scenarios.

The most prevalent refractivity feature over the ocean is the evaporation duct, which occurs due to the rapid decrease in humidity just above the ocean surface. This effect results in a ducting layer with a height of 0 to 40 meters (0 to 130 feet). Statistical distributions for the occurrence of evaporation duct heights as a function of geographic location are available in Reference 5. The evaporation duct does not exist over land

(except perhaps marsh/swamp areas). Generally, only frequencies above 1 GHz are significantly affected by this feature.

Surface-based ducts are typically caused by the advection of warm dry air from land over the moist marine boundary layer, resulting in an elevated temperature inversion and the trapping of moisture below the inversion. The resulting trapping/ducting layer may occur anywhere from very near the surface to a height of 500m (1500 ft). Trapping layers at higher altitudes usually result in elevated ducts. For the LSLT situation, surface-based ducts may or may not increase power on the target, but these conditions can drastically increase the strength of land clutter returns from as far away as several hundred miles. Surface-based ducts may persist over land, but their behavior inland from the coast is difficult to predict. Average surface-based duct heights and thicknesses are also available, referenced to location and month, in Reference 5. All frequencies above a few hundred MHz are affected by surface-based ducting.

Elevated ducts are caused by the same phenomenology as surface-based ducts, but energy trapped in elevated ducts does not reach the surface. The effects of elevated ducts will be most severe when the trapping layer is located at or just above the sensor, and the target of interest is at a similar altitude (HSHT situation) (Reference 6).

Subrefraction results when warm moist air flows over a cooler ocean or cool dry air. In severe cases, the refractive index will increase with altitude and effective earth radii of less than 1 are possible. Excellent examples of this situation are given in References 2, 3, and 4. Although, this effect is most important for surface-based systems, subrefractive layers can also occur at higher altitudes, thus having some impact on the HSHT case. Presently, probabilities of occurrence for subrefraction in areas other than the U.S. Mid-Atlantic region are unknown. Subrefractive layers are often deep enough (large enough) to impact most frequencies of interest.

There are a few rules regarding which of the above conditions can exist concurrently. The presence of subrefraction rules out evaporation ducting, but not necessarily surface-based ducting; that is, a subrefractive layer attached to the sea surface may be "capped" by a strong trapping layer. On the other hand, evaporative and surface-based ducts may exist simultaneously. The joint probabilities and correlations of these conditions are unknown.

Finally, refractive conditions can vary significantly with range and azimuth, particularly in coastal environments. Although these variations can impact observed and predicted performance, lateral variability is usually not considered except for specific cases for which atmospheric data have been collected; e.g., during well-instrumented Navy tests. Lateral homogeneity is typically assumed for design studies.

C.3.0 DIFFRACTION

The two situations involving diffraction effects are performance near and beyond the spherical earth horizon (spherical earth diffraction), and near and behind terrain features. In the latter case, the diffraction is related to what is commonly referred to as terrain blockage. The details of how energy propagates beyond the horizon and/or behind land features impacts both power on target and monostatic and bistatic clutter. Depending on the maximum coverage range required, the horizon limit may be important for an elevated sensor. Similarly, depending on the operating altitude and range, an elevated sensor will also experience blockage-related diffraction, although it will be substantially less than for surface-based sensors. Diffraction effects in land clutter modeling are discussed in Reference 7.

C.4.0 PRECIPITATION AND DUST

Precipitation introduces some amount of loss due to absorption and/or scattering at all frequencies above 1 GHz for sufficiently large precipitation rates. Attenuation versus frequency and rain rate can be calculated following the procedure given in Section A.2.8.

Stratiform precipitation can exist uniformly up to nominally 4 km (13 kft) (Section A.2.3.2.1), so losses should be assumed to occur at any point at which a rain cell is intersected by the slant path from sensor to the point of interest. For the higher rain rates, however, the rain will not be uniform over large lateral regions; that is, the cells have decreasing diameters for increasing rain rates (Reference 8). Discussion of lateral spatial distribution versus rain rate is provided in Section A.2.4.

Attenuation through clouds may be significant at frequencies above 10 GHz (References 9 and 10). The degree of attenuation will depend on the temperature and water vapor content of the cloud, as well as frequency. The method of calculating cloud attenuation is provided in Section A.3.8.

Substantial attenuation through dust storms may be experienced in certain regions, such as the Arabian Gulf. Although microwave attenuation through clouds of well-characterized dust particles is well understood, the physical parameters of natural dust storms, such as size, particle density, and number distribution, are not. References for recent work in this area are collected in Reference 11. Previous studies have assumed dust storm dimensions of 18.5 km (10 nmi) in lateral extent and uniform density between the surface and 1.5 km (5 kft). Typical size distributions and number densities give S-band and X-band attenuations of approximately 0.2 and 0.65 dB/km, respectively, through the storm. The attenuation increases linearly with frequency. Further work is needed to establish spatial extents and particle size distributions for realistic dust storms.

A1A97U-070

C.5.0 GASEOUS ABSORPTION

Absorption due to oxygen and gaseous water vapor can be significant over long paths. Figure C.5-1 provides plots of the one-way attenuation coefficient versus frequency for oxygen and water vapor (Reference 9).
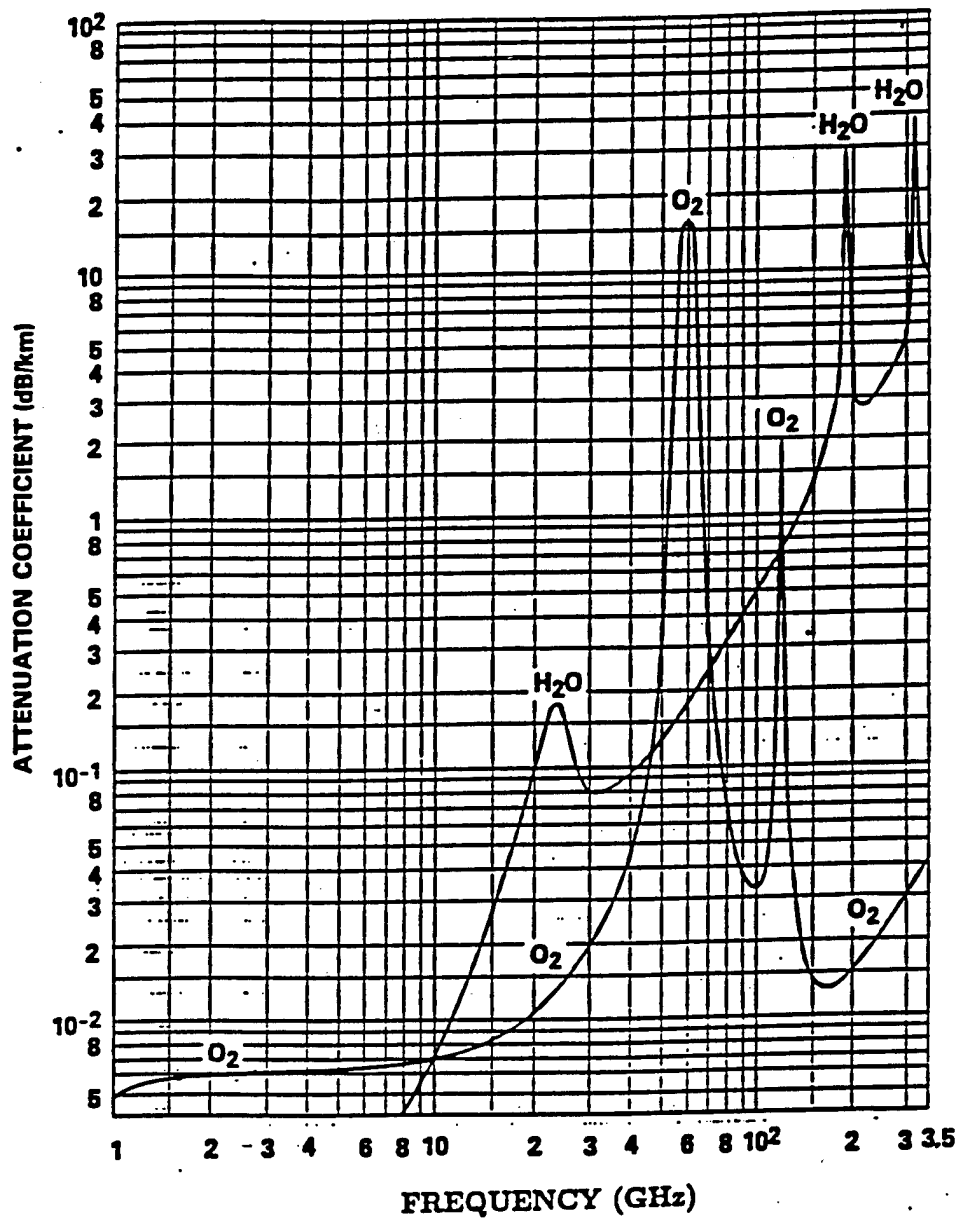
Figure C.5-1 Atmospheric Gaseous Absorption

For frequencies at which both components are appreciable, the two attenuation coefficients should be added to obtain the total attenuation. The absorption coefficients in Figure C.5-1 (sea level, water vapor of 7.5 g/m^3, and temperature of 15 °C) should be assumed along the entire propagation path.

Gaseous absorption may be calculated using the methods specified in the CCIR (Reference 9). For a terrestrial path, or for slightly inclined paths close to the ground, the one-way path attenuation may be written as

$$A_a = \gamma_a r_0 = \left(\gamma_o + \gamma_w\right)r_0 \qquad dB$$

where

$r_0 = $ path length (km)

$\gamma_a = $ specific attenuation (dB/km)

$\gamma_o = $ dry air contribution (dB/km)

$\gamma_w = $ water vapor contribution (dB/km).

For dry air, the specific attenuation at ground level (pressure = 1013 mb) and at a temperature of 15° C is mainly due to oxygen and is given by

$$\gamma_o = \left[7.19 \times 10^{-3} + \frac{6.09}{f^2 + 0.227} + \frac{4.81}{(f-57)^2 + 1.50}\right] f^2 \times 10^{-3} \quad dB/km$$

for $f < 57$ GHz.

For water vapor, the specific attenuation at sea level, at a temperature of 15° C, and including the effects of the quadratic dependence on water vapor density, is given by

$$\gamma_w = \left\{0.05 + 0.0021\rho + \frac{3.6}{(f-22.2)^2 + 8.5} + \frac{10.6}{(f-183.3)^2 + 9.0} + \frac{8.9}{(f-325.4)^2 + 26.3}\right\} f^2 \rho 10^{-4} \quad dB/km$$

for $f < 350$ GHz

where f is the frequency expressed in GHz, and ρ is the water vapor density expressed in g/m^3. As previously mentioned, a value of $\rho = 7.5 g/m^3$ should be used in the above equation.

C.6.0 MULTIPATH INTERFERENCE

Both specular and diffuse multipath affect target signal reception as a function of polarization, grazing angle, frequency, surface roughness, and surface characteristics*. This section describes a method for calculating specular multipath effects under "standard atmosphere" conditions. Section B includes a discussion of diffuse multipath effects. Commentary and cautionary notes are appropriate for some portions of this model, as denoted by an asterisk, *, following the applicable text.

C.6.1 Pattern Propagation Factor

Calculation of the pattern propagation factor for the multipath interference region is covered in Chapter 6 of Reference 12 in the section entitled "The Pattern Propagation Factor," pg. 239. The following multipath effects are included in high fidelity propagation models, such as TEMPER, and should also be included in any spherical-earth model that is chosen.

The one way propagation factor in the presence of specular multipath reflection is given by

$$F^2 = 1 + R^2 + 2R \cos\left(\Delta\phi\right)$$

where the relative magnitude of the specular reflection is given by

$$R = D\left(\Delta G\right) \rho_o \rho_s \ ,$$

the phase shift of the specular reflection is given by

$$\Delta\phi = \left(2\pi\Delta r / \lambda\right) + \phi_o \ ,$$

the divergence factor is given by

$$D = \left[1 + \frac{4r_1 r_2}{a_e r \sin\left(2\psi\right)}\right]^{-\frac{1}{2}} \ ,$$

and ΔG = antenna gain ratio between the specular point direction and the target,

   r_1 = slant range between radar and specular point,

   r_2 = slant range between specular point and target,

   r = slant range between radar and target,

   $\Delta r = r_1 + r_2 - r$ = path length difference between the indirect and direct paths,

ρ_o = magnitude of the complex Fresnel reflection coefficient,

ϕ_o = phase of the complex Fresnel reflection coefficient*,

ρ_s = rough surface specular reflection coefficient,

ψ = grazing angle,

a_e = effective radius of the earth (4/3 physical radius), and

λ = radar wavelength.

Diffuse reflection effects can be modeled separately using the expressions in Section B.3.0 concerning bistatic forward scatter.

C.6.2 Multipath Geometry

Multipath geometry is discussed in Reference 12 in the section entitled "Less Restrictive Spherical-Earth Solution," pg. 253. The formulas in this section are for search radar applications using an effective earth radius diffraction model.

C. 6.3 Reflection Coefficients

C.6.3.1 Fresnel Reflection Coefficient

The complex electromagnetic reflection coefficient* is discussed in Reference 12 in the section entitled "Electromagnetic Reflection Coefficient," pg. 258. The complex Fresnel reflection coefficient for horizontal polarization is given by

$$\rho_o \exp(-j\phi_o) = \frac{\sin\psi - \sqrt{\varepsilon_c - \cos^2\psi}}{\sin\psi + \sqrt{\varepsilon_c - \cos^2\psi}}$$

The complex Fresnel reflection coefficient for vertical polarization is given by

$$\rho_o \exp(-j\phi_o) = \frac{\varepsilon_c \sin\psi - \sqrt{\varepsilon_c - \cos^2\psi}}{\varepsilon_c \sin\psi + \sqrt{\varepsilon_c - \cos^2\psi}}$$

where ε_c is the complex dielectric constant*,

$$\varepsilon_c = \varepsilon_r - j60\lambda\sigma$$

and

ε_r = dielectric constant (relative permittivity)

σ = conductivity (mho/m)

λ = radar wavelength (m)

$j = \sqrt{-1}$.

Sea Water

The complex dielectric constant* for sea water (Reference 13) is given by

$$\varepsilon_c = \varepsilon_r - j\varepsilon_i$$

where

$$\varepsilon_r = \frac{\varepsilon_s - \varepsilon_o}{1 + x^2} + \varepsilon_o$$

$$\varepsilon_i = (\varepsilon_r - \varepsilon_o)x + \frac{2\sigma_i}{f}$$

$$x = 2\pi f\tau.$$

with

f = RF frequency (Hz),
ε_o = reference value of dielectric constant,
ε_s = static dielectric constant,
σ_i = ionic conductivity, and
τ = relaxation constant.

Dielectric constant parameters are given in Table C.6-1 for various sea temperatures assuming a salinity of 36 parts per thousand (Reference 14). Reference 15 suggests the parameters for a 10°C sea temperature as typical.

Table C.6-1   Sea Water Dielectric Constant Parameters

	T = 0°C	T = 10°C	T = 20°C
ε_s	77.57	75.41	72.26
ε_o	4.9	4.9	4.9
τ	17.03×10^{-12}	12.25×10^{-12}	9.08×10^{-12}
σ_i	2.68×10^{10}	3.51×10^{10}	4.41×10^{10}

Examples of the Fresnel reflection coefficients for sea water are presented in Figure C.6-1. This plot shows the magnitudes and phases of the reflection coefficients for horizontal and vertical polarizations as a function of grazing angle and frequency. A plot of the phase for horizontal polarization is not given because it is almost exactly (π) radians for the range of angles and frequencies plotted.
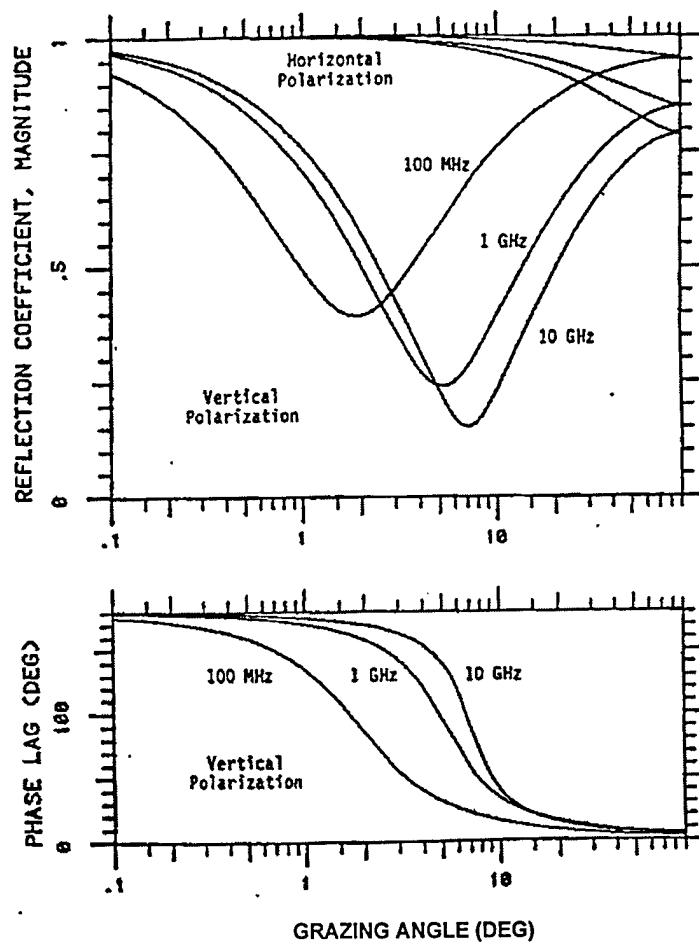

Figure C.6-1 Fresnel Reflection Coefficients for Sea Water

Land

The complex dielectric constant for land depends on the type of land cover. In the following discussion, land cover is divided into six classes :

(1) barren land,
(2) range land,
(3) wet land,
(4) forest,
(5) agricultural, and
(6) urban.

Barren land and range land are considered to be made up of a mixture of soil and water. The dielectric constant is computed from the percentage of water by volume as described below. Barren land is assumed to have 5% water by volume and range land 15%. These values were chosen to match the computed model values for the dielectric constant with data contained in Kerr (Reference 16) and Meeks (Reference 17).

Wet land, forest, and agricultural land are assumed to be covered with vegetation containing water. Wet land is assumed to have 90% water by weight, forest 40%, and agricultural land 50%. The dielectric constant is computed from the percentage of water by weight in the vegetation. These percentages of water were chosen based on the guidance provided in Ruck (Reference 18) that the percentage of water in vegetation varies from 30% in very dry grass to 90% in wet grass. Urban surfaces are assumed to be covered by asphalt.

Complex Dielectric Constant for Soil Containing Water

Values for the complex dielectric constant of soil containing water, derived from References 16 and 17, are used for the barren and range land categories. These data were fit with a linear approximation as a function of fraction of water by volume. This approximation is

$$\varepsilon_s = b_o + m_1(\lambda) \cdot f_w + j\, m_2(\lambda) \cdot f_w = \varepsilon_s^{(1)} + j\, \varepsilon_s^{(2)}$$

where

$$m_1(\lambda) = A_1(\lambda) \cdot \varepsilon_w^{(1)}(\lambda)$$
$$m_2(\lambda) = A_2(\lambda) \cdot \varepsilon_w^{(2)}(\lambda)$$
$$b_o = 2.75$$

with

$$A_1(\lambda) = 0.45 + (0.015) \cdot f_{GHz}$$
$$A_2(\lambda) = 0.35 + (0.017) \cdot f_{GHz}$$

$$\varepsilon_w = \varepsilon_w^{(1)} + j\,\varepsilon_w^{(2)} = 5 + 75/(1 + j \cdot (1.85/\lambda)) \quad (\lambda \text{ in cm, Reference 19})*$$

and

f_{GHz} = RF frequency, GHz
f_w = fraction of water by volume
ε_s = complex dielectric constant of soil
ε_w = complex dielectric constant of water
λ = RF wavelength (cm).

For barren land, $f_w = 0.05$; for range land, $f_w = 0.15$. Results from this approximation are given in Table C.6-2.

Table C.6-2   Electromagnetic Properties of Soil from Approximation

Frequency (GHz)	Moisture Content by Volume							
	0.3%		10%		20%		30%	
	$\varepsilon_s^{(1)}$	$\varepsilon_s^{(2)}$	$\varepsilon_s^{(1)}$	$\varepsilon_s^{(2)}$	$\varepsilon_s^{(1)}$	$\varepsilon_s^{(2)}$	$\varepsilon_s^{(1)}$	$\varepsilon_s^{(2)}$
0.3	2.9	0.002	6.4	0.05	10.0	0.1	13.7	0.2
3.0	2.9	0.016	6.6	0.54	10.4	1.1	14.3	1.6
8.0	2.8	0.043	6.5	1.45	10.2	2.9	13.9	4.3
14.0	2.8	0.065	5.9	2.18	9.1	4.3	12.2	6.5
24.0	2.8	0.079	5.1	2.64	7.4	5.3	9.7	7.9

Complex Dielectric Constant for Vegetation Containing Water

The complex dielectric constant for vegetation containing water, which is used for the wet land, forest, and agricultural land cover categories (Reference 18) is modeled by

$$\varepsilon_v = \varepsilon_v^{(1)} + j\,\varepsilon_v^{(2)} = 2.5 \cdot (1-f) + f \cdot \varepsilon_w$$

where

$$\varepsilon_w = 5 + 75/(1 + j \cdot (1.85/\lambda)) \qquad (\lambda \text{ in cm})*$$

and

$\quad$ f $\ =$ fraction of water by weight

$\quad$ ε_v $\ =$ complex dielectric constant of vegetation

$\quad$ ε_w = complex dielectric constant of water.

$\quad$ λ $\ =$ RF wavelength (cm).

For forest, agricultural, and wet land, $f = 0.4, 0.5$, and 0.9 respectively.

Complex Dielectric Constant for Asphalt

$\quad$ The formula used for the complex dielectric constant* of asphalt (Reference 19), which is used for the urban land cover category, is

$$\varepsilon_a = b_a + m_a\, f_{MHz} - j\, a\, f_{MHz}^2$$

where

$$a\ = 1.3125 \times 10^{-9}$$
$$b_a = 6.1$$
$$m_a = -1.8 \times 10^{-4}$$

and

$$f_{MHz} = \text{RF frequency in MHz.}$$

This formula was chosen to fit data at X band and K_a band for a dielectric constant of

$$\varepsilon_v = 4.3 - j\, 0.1 \qquad \text{(X band)}$$
$$\varepsilon_v = 2.5 - j\, 0.65 \qquad (K_a \text{ band}).$$

C.6.3.2 Rough Surface Reflection Coefficient

$\quad$ The specular reflection coefficient will be very small except for localized areas where the average terrain slope gives near-zero grazing in a particular resolution cell. This condition occurs over the crests of hills and mountains. In this cell, specular enhancement or degradation can occur. More generally, the overall propagation factor will have a random nature which, in the simplest modeling approaches, can be approximated assuming a diffuse reflection coefficient which represents the $\pm$ one sigma bound on propagation. Further details about modeling diffuse reflection effects may be found in Section B.3.0.

The specular coefficient depends on the surface roughness, grazing angle, and RF frequency. The following equations for reflection coefficient were taken from Reference 20. The rough surface specular reflection coefficient (Miller-Brown-Vegh model) is given by

$$\rho_s = (\exp(-2(2\pi g)^2))I_0(2(2\pi g)^2)$$

where

$$g = \frac{\sigma_h \sin\psi}{\lambda}$$

σ_h = RMS deviation from a smooth surface (m),

I_0 = modified Bessel function, $J_0(jx)$.

Standard Deviation of Sea Surface Height

The standard deviation of the sea surface is defined in terms of the sea state, as follows,

$$\sigma_h = (0.0118)\, A_s^{2.6}$$

where

A_s = sea state number for sea state defined by the World Meteorological Organization, and

σ_h = standard deviation of surface height (m).

Standard Deviation of Land Surface Height

Two parameters are used to describe the standard deviation of land surfaces. These are the land form and land cover. The standard deviation of the land surface is assumed to be the root sum square of the contributions from the land form and land cover, i.e.,

$$\sigma_h = (\sigma_{hf}^2 + \sigma_{hc}^2)^{\frac{1}{2}}$$

where

σ_{hf} = standard deviation contribution due to land form (m), and

σ_{hc} = standard deviation contribution due to land cover (m).

Five land form and six land cover types are defined. The land form and land cover types and the surface height standard deviation (σ_h) are given in Table C.6-3 and Table C.6-4 from References 12, 21, and 22.

Table C.6-3   Land Form Height Standard Deviation

Land Form	σ_{hf} (m)
Level	5.0
Undulating	10.0
Hummocky	20.0
Rolling	60.0
Mountains	150.0

Table C.6-4   Land Cover Height Standard Deviation

Land Cover	σ_{hc} (m)
Barren Land	0.001
Range Land	0.25
Wet Land	0.25
Forest	3.0
Agricultural	0.1
Urban	20.0

C.6.4 Commentary and Cautionary Notes

C.6.4.1 Multipath Models

When high-fidelity simulations of monopulse tracking and/or active and semi-active missile seeker operation are needed, fine-scale shadowing, multipath from "out-of-plane" scatterers and other detailed effects may have to be included. Although considerable work has been done in these areas, standardized methods and models for a particular application do not presently exist. Examples can be found in References 23 and 24. Similar effects can also be important when modeling operation against terrain bounce jammers, as discussed in Reference 23, Section 10.

C.6.4.2 Fresnel Reflection Coefficients

Sign conventions concerning the phase of the Fresnel reflection coefficient differ in the literature. The convention used herein is that of Kerr (Reference 16). A positive value of ϕ_0 denotes a phase lag. This convention requires that the imaginary part of the complex dielectric constant be negative. The phase contribution of the dielectric material upon reflection is equivalent to an extension of path length, resulting in additional phase lag. Some of the equations for complex dielectric constant presented herein have been modified to reflect this convention.

A1A97U-070

C.7.0 HIGH FIDELITY PROPAGATION MODELS

High fidelity propagation models based on the parabolic approximation to the Helmholtz wave equation intrinsically include the effects of refraction, diffraction, and forward surface reflections (coherent multipath). Two available models which are frequently used are RPO (Radio Physical Optics) (Reference 25) and TEMPER (Tropospheric Electromagnetic Parabolic Equation Routine) (References 26 and 27). RPO was developed by the Naval Communications, Control and Ocean Surveillance Center Research, Development, Test & Evaluation Division (NCCOSC RDT&E, or NRaD). TEMPER was developed by The Johns Hopkins University Applied Physics Laboratory.

RPO is a Navy-certified hybrid model that uses the parabolic wave equation for low angles where refractive effects are important. Unfortunately, RPO does not accommodate terrain or transmit antenna heights above 100 meters (328 ft), and RPO's surface roughness algorithm is inaccurate. RPO is currently being upgraded to rectify these limitations, but the completion date for these improvements is not until early 1998. Terrain capability is being added by merging RPO with another NRaD propagation model called TPEM (Terrain Parabolic Equation Model) (Reference 28).

TEMPER accommodates terrain, surface roughness and high-altitude antennas, although execution times can be substantial for long-range, high-altitude problems at high frequencies. TEMPER should be used to calculate the propagation factor associated with the target return and surface scattering (forward and backward) for radars and illuminators in the following circumstances :

1. Any geometry involving propagation paths at angles less than 1.5 degrees relative to the local horizontal. Such geometries are sensitive to refractive effects.

2. Any geometry leading to diffraction and shadowing behind terrain features, independent of the importance of refraction.

Situations in which alternative propagation models, such as the spherical-earth model (Sections C.6.1 and C.6.2), may be used are:

1. Surface-to-air and air-to-air propagation paths at angles greater than 1.5 degrees relative to the local horizontal.

2. Short range (less than 10 km) paths not in the vicinity of terrain blockage.

None of the parabolic equation propagation models are validated for frequencies above 20 GHz. The hope is that for higher frequencies, the path lengths will be short enough to allow refractive effects to be neglected. Furthermore, above 20 GHz,

diffraction may be ignored in favor of simple optical blockage calculations. Alternative methods to calculate diffraction, such as GTD (geometric theory of diffraction) and UTD (unified theory of diffraction), may also be used for Ka-band and above.

The existing parabolic equation (PE) models represent the coherent portion of the forward scatter from the sea or land surface (multipath) using the standard Fresnel reflection coefficient formalism. Non-coherent (diffuse) scattering is neglected by PE models except to the degree that it results in reduced power in the coherent reflection. These models also assume continuous wave (CW) propagation, which for elevated pulsed sensors may pose a problem. The issue of properly representing pulsed systems using CW models is discussed in Reference 6. As a rule, however, use of CW models for target altitudes that are within a few hundred feet of the surface will produce the correct results, even for elevated pulsed systems.

The typical source of terrain height data for terrain propagation calculations is the Digital Terrain Elevation Database (DTED) (Reference 29). TEMPER accepts a simple array of terrain height versus range as an input.

Models for gaseous absorption and attenuation due to precipitation may or may not be included in existing propagation codes. Since these losses are easily calculated and added separately, they should be determined using the information provided in Sections C.4.0 and C.5.0.

C.8.0 REFERENCES

1. M. I. Skolnik, *Radar Handbook*, New York: McGraw-Hill, 1970, Chapter 24.
2. J. Goldhirsh, et al, "Three years of C band signal measurements for overwater, line-of-sight links in the mid-Atlantic coast: 1. Fade statistics," *Radio Science*, Vol. 29, No. 6, pp. 1421-1431, 1994.
3. J. Goldhirsh, et al, "Three years of C band signal measurements for overwater, line-of-sight links in the mid-Atlantic coast: 2. Meteorological aspects of sustained deep fades," *Radio Science*, Vol. 29, No. 6, pp. 1433-1447, 1994.
4. J. Stapleton and S. Kang, "Ku-Band Propagation Measurements in the Low Altitude Region," NSWC/Dahlgren Division Report NSWCDD/TR-95-66.
5. Ducting Climatology Summary (DCS), Version 2.0, 21 January 1992, Available from NRaD via internet at "http://sunspot.nosc.mil/543".
6. M. H. Newkirk, "Propagation Effects for High-Altitude Radiating Systems," JHU/APL memorandum F2F-96-U-4-008, 9 September 1996.
7. J. P. Reilly and C. C. Lin, "Radar Terrain Effects Modeling for Shipboard Radar Applications," JHU/APL report FS-95-060, April 1995.
8. J. Goldhirsh and B. H. Musiani, "Dimension Statistics of Rain Cell Cores and Associated Rate Isopleths Derived from Radar Measurements in the Mid-Atlantic Coast of the United States," *IEEE Trans. on Geoscience and Remote Sensing*, Vol. 30, No. 1, pp. 28-37, 1992.
9. CCIR (International Radio Consultive Committee), "Recommendations and Reports of the CCIR, 1990," Vol. V-5, Propagation in Non-Ionized Media, XVIIth Plenary Assembly, Dusseldorf, 1990.
10. K. L. S. Gunn and T. W. R. East, "The Microwave Properties of Precipitation Particles," *Quarterly Journal of Royal Meteorological Society*, Vol. 80, pp. 522-545, 1954.
11. R. V. Biordi, "Effect of Sand/Dust Particles on Microwave Propagation: Compendium," JHU/APL Report STD-N-854, September 1991.
12. Blake, L. V., *Radar Range-Performance Analysis*, D. C. Heath & Co. (Lexington Books), Lexington, MA, 1980.
13. J. A. Saxton and J. A. Lane, "Electrical Properties of Sea Water," *Wireless Engineer*, October 1952, pp. 269-275.
14. Klein, L. A., and Swift, C. T., "An Improved Model for the Dielectric Constant of Sea Water at Microwave Frequencies," *IEEE Transactions on Antennas and Propagation*, Vol. AP-25, No.1, January 1977.
15. *Radar Workstation Manual, Volume II, Functional Description*, Technology Services Corporation, 1988.
16. Kerr, D. E., ed., *Propagation of Short Radio Waves*, McGraw-Hill, New York, 1951 (Volume 13 of the MIT Radiation Laboratory Series). Republished by Dover Publications, Inc., New York, 1965.

17. Meeks, M., *Radar Propagation at Low Altitudes*, Artech, Dedham, MA, 1982.

18. Ruck, G., Ed., *Radar Cross-Section Handbook*, Vol. 2, 1970.

19. Cosgriff, R.L., Peake, W.H., and Taylor, R.C., "Terrain Scattering Properties for Sensor System Design (Terrain Handbook II)," The Ohio State University Antenna Laboratory, May 1960, Reprinted in Barton, D.K., *Radars Volume 5, Radar Clutter*, Artech, 1975.

20. Miller, A. R.; Brown, R. M.; Vegh, E., "New Derivation for the Rough-Surface Reflection Coefficient and for the Distribution of Sea-Wave Elevations," *IEE Proceedings*, Vol. 131, Pt. H, No.2, Apr 1984.

21. Billingsley, J., "Tabulated Radar Ground Clutter Amplitude Statistics by Terrain Classification," MIT Lincoln Laboratory, 48PM-CMT-0009,1 September 1982.

22. Longley, A., and Rice, P., "Predictions of Troposphere Radio Transmission Loss over Irregular Terrain, a Computer Method," ESSA Technical Report ERL 79-ITS-67, July 1968.

23. Osborne, John H., "NSWCDD Proposed Multipath Model For The Close-In Weapons System (CIWS)," NSWCDD/TR-92/35, February 1992, NSWCDD, Dahlgren VA.

24. Macfadzean, R., *Surface-Based Air Defense System Analysis*, Sections 7.5 and 7.6, 1992, Artech.

25. H. V. Hitney, "Hybrid Ray Optics and Parabolic Equation Methods for Radar Propagation Modeling," *Proc. IEE Int. Conf. Radar*, Brighton, U.K., Oct. 12-13, No. 365, pp. 54-57, 1992.

26. G. D. Dockery, "Description and Validation of the Electromagnetic Parabolic Equation Propagation Model (EMPE)," JHU/APL Report FS-87-152, September 1987.

27. G. D. Dockery and J. R. Kuttler, "An Improved Impedance-Boundary Algorithm for Fourier Split-Step Solutions of the Parabolic Wave Equation," *IEEE Trans. on Antennas and Propagation*, Vol. 44, No. 12, pp. 1592-1599, 1996.

28. A. E. Barrios, "A Terrain Parabolic Equation Model for Propagation in the Troposphere," *IEEE Trans. on Antennas and Propagation*, Vol. 42, No. 1, pp. 90-98, 1994.

29. "Catalog of Maps, Charts, and Related Products, Part 7, Digital Data Products, Vol. I, Terrain and Feature Data," Defense Mapping Agency, DMA Stock #CATP&VO1.